AN ABSTRACT OF THE THESIS OF

John L. Sharp for the degree of Master of Science in Oceanography presented on February 8, 1991.
Title: Manganese and Iron Geochemistry in the Endeavour Ridge Hydrothermal Plume.

Redacted for privacy

Abstract approved: _____
Robert W. Collier

Extensive CTD (conductivity-temperature-depth) hydrocasts were conducted over the Endeavour Segment of the Juan de Fuca Ridge in June, 1988 to determine the removal rates of manganese and iron from hydrothermal plumes. Approximately 100 trace metal samples were taken in the neutrally buoyant plume at 10 locations ranging from the vent field to 17 km "downplume." These samples were analyzed for both total and dissolved manganese and iron.

The Mn/ΔT ratio of the neutrally buoyant plume over the vent field is similar to the Mn/ΔT ratio of the high-temperature vents at Endeavour Ridge. Based on excess temperature, or ΔT, as a conservative tracer of the high-temperature end-member solution, this observation supports the view that little manganese is lost during the buoyant rise of the plume. However, as the plume advects away from the vent field, the Mn/ΔT ratio decreases. Manganese is oxidized at a rate of ~1.3 x 10^{-11} moles Mn/kg/hr, which is consistent with bacterial oxidation rates. The bacterial morphology of the plume samples changes from ~1 μm cocci at the vent field to 10 -15 μm filamentous, sheathed bacteria at the 17-km stations.

Iron is oxidized from Fe(II) to Fe(III) very rapidly near the vent field. Total iron is removed from solution at higher rates near the vent field, with the removal rate decreasing away from the vent field. The overall Fe/Mn ratio of the particles that are removed from the plume

during its advection from the vent field to the 17-km stations is 5:1, within the characteristic range observed in hydrothermal sediments.

Iron and light absorbance are correlated at distances of 2 km or greater from the vent field. However, at the vent field, light absorbance exceeds the values predicted by the far-field relationship. This increased absorbance appears to be due to an increased population of particles smaller than 0.4 μm. These submicron diameter particles are aggregated and removed quickly as the plume advects away from the vent field.

Manganese and Iron Geochemistry in the Endeavour Ridge Hydrothermal Plume

by

John L. Sharp

A THESIS

submitted to

Oregon State University

in partial fulfillment of
the requirements for the
degree of

Master of Science

Completed February 8, 1991
Commencement June 1991

APPROVED:

Redacted for privacy

Professor of Oceanography in charge of major

Redacted for privacy

Dean of College of Oceanography

Redacted for privacy

Dean of Graduate School

Date thesis is presented February 8, 1991

Typed by John L. Sharp

ACKNOWLEDGEMENT

I would like to thank Bob Collier for both financial support and philosophical and technical advice for the past three and a half years. It would be difficult to imagine a better advisor. He greatly reduced the "scatter" in my thoughts, allowing greater concentration. Marv Lilley and John Baross did the bacterial work presented in this thesis, which greatly improved the quality of the findings. I would like to thank Russ McDuff and Dave Butterfield for being so helpful and unselfish in sharing their data and models. I would also like to thank Gary Klinkhammer, James Cowen, and Andy Campbell for reviewing previous manuscripts. Thanks also to the rest of my committee: Jack Dymond, Pete Nelson, and Dave Myrold.

I would especially like to thank Chi Meredith, both for doing the iron analyses and for being a great office-mate. Special thanks also to Jim McManus for helping me wash about 1000 bottles, and making me laugh during some very frustrating times. We never solved the world's problems, but we did argue about them alot. I would also like to thank Jim Robbins for helping me with some very exasperating experiments. They never worked, but the experience was invaluable.

I would also like to thank my parents who must continually wonder if their child could have been switched in the hospital ward. I just have itchy feet and a curious mind. Most of all, I would like to thank my fiance, Anne, for helping me keep things in perspective. She, along with Jimmy Buffett, Mark Twain, Barbara Tuchman, James Burke, W. A. Mozart, Yo-Yo Ma, and Andrew Lloyd Webber, helped me realize that there are things in life other than hydrothermal plumes.

TABLE OF CONTENTS

LIST OF FIGURES

LIST OF FIGURES

LIST OF FIGURES

LIST OF FIGURES

LIST OF TABLES

Manganese and Iron Geochemistry in the Endeavour Ridge Hydrothermal Plume

INTRODUCTION

"One is often surprised at the juvenilities which grown people indulge in at sea, and the interest they take in them, and the consuming enjoyment they get out of them."

Mark Twain
Following the Equator

Oceanographers spend their days trying to find out what seawater is, what is in it, how did it get there, and where does it go? They try to develop balances between inputs, such as riverine and atmospheric, and outputs, such as deep-sea sediments. This gives a basic idea of the "cycling" of elements. The discovery of hydrothermal vent fields on the mid-ocean ridges during the 1970's gave oceanographers a greater understanding of the cycles of magnesium and manganese. Previous to this discovery, oceanographers could not find all of the inputs of manganese nor all of the outputs of magnesium. Hydrothermal vent fields provided the answers.

At oceanic spreading centers, seawater seeps into the seafloor through cracks and fissures in the newly created basaltic crust. During the time the water is below the seafloor, it loses magnesium and sulfate to the crust, and gains various trace elements, magmatic volatiles, and heat from the crust. Depending on the depth of the penetration and the degree of subsurface mixing with ambient seawater, the hydrothermal solutions emerge from the seafloor at temperatures ranging from approximately 2° C to ~350° - 400° C. The high-temperature solutions

are enriched approximately 10^6 times in iron and manganese relative to normal oceanic concentrations (Von Damm and Bischoff, 1987; Von Damm, et al., 1985a; Von Damm, et al., 1985b). In fact, hydrothermal vent fields are the major sources of iron and manganese to the deep ocean. These fluids form buoyant plumes that rise and entrain surrounding seawater, until a level of neutral buoyancy is reached. This level is appproximately 200 meters above the seafloor in the Pacific Ocean and 350 meters above the seafloor in the Atlantic Ocean (Speer and Rona, 1989).

In contrast to the high-temperature fluids, the lower temperature fluids do not have the buoyancy flux necessary to rise to these heights in the water column. However, the low-temperature fluids may modify the properties of the water entrained by the high-temperature fluids. Recent studies show that the total heat flux from low-temperature, diffuse flows may be approximately an order of magnitude greater than that from high-temperature vents at both the ASHES vent field on Axial Volcano on the southern Juan de Fuca Ridge (Rona and Trivett, 1990) and at the Endeavour Ridge vent field on the northern Juan de Fuca Ridge (Schultz, et al., 1990).

After achieving a level of neutral buoyancy, the combined vent water and entrained water are advected horizontally by the prevailing currents. Stommel (1982) has suggested that hydrothermal systems may actually drive oceanic circulation cells. The neutrally buoyant plumes contain chemical and physical anomalies such as decreased light transmission, high concentrations of iron, manganese, ^{3}He, methane, hydrogen, and radon. In the Pacific Ocean, plumes have increased heat and salt content relative to the water normally found at the depth of the plumes. Since ^{3}He concentration and heat content are conservative (Lupton, et al., 1989), any decrease in these properties due to mixing rather than chemical reaction or removal by scavenging. Thus, they provide a measure of the dilution of the neutrally buoyant plume and allow the estimation of the rates of removal of the non-conservative chemical constituents. Previous research has been focused on estimating and explaining the rates and mechanisms of removal of methane and hydrogen (Angelis, 1989; Kadko, et al., 1990; Lilley, et al., 1983;

Welhan and Craig, 1983; Winn, et al., 1986), organic compounds (Roth and Dymond, 1989), and iron and manganese (Campbell, et al., 1988; Cowen, et al., 1986; Cowen, et al., 1990; Kadko, et al., 1990; Lupton, et al., 1980; Massoth, et al., 1984; Mottl and McConachy, 1990; Trocine and Trefry, 1988; Weiss, 1977).

In this thesis, I present a study undertaken to determine the rates of removal of iron and manganese from the Endeavour Ridge hydrothermal plume in the northeast Pacific Ocean. The results are compared to previous research on the composition of the vent fluids and the composition of hydrothermally-influenced sediments.

METHODS

I. Precruise Preparation

250-ml and 500-ml polyethylene sample bottles were cleaned by filing them with 1 N HCl and heating at ~80° C for 3 days. The bottles were then rinsed 3 times with Milli-Q® water and air-dried under a Class 100 laminar-flow hood. The bottles were capped, covered with a polyethylene glove, and placed in plastic bags in groups of 12. Nuclepore® polycarbonate filters (47-mm, 0.4 μm pore diameter), filter assemblies, and teflon tweezers used for handling filters were stored in 0.5 N HCl until time of use. The apparatus for drawing samples from the Niskin® bottles was soaked in 1 N HCl for 3 days, rinsed with Milli-Q® water, and air-dried under a Class 100 laminar flow hood.

II. Shipboard Procedures

The location of the stations occupied during the June, 1988 cruise and the local bathymetry of Endeavour Ridge are shown in Figure 1. The exact station locations are listed in Table 1. The stations were occupied according to the numerical suffix in the hydrocast identifier (i.e., P2CTD1 was the first hydrocast and P2CTD15 was the 15th hydrocast). The water column at the vent field was sampled 4 times throughout the cruise's duration, in order to evaluate short-term geochemical variations. Stations were occupied at the vent field, and 2 km, 4 km, 10 km, and 17 km "downplume". The orientation of the plume was determined by a series of hydrocasts and "tow-yos" at the beginning of the cruise. A "tow-yo" is a hydrocast in which the CTD instrument package is raised and lowered through the water column while the ship is underway slowly. This technique gives a better idea of the orientation of the plume than does a single vertical hydrocast. A station was also sampled 10 km east of the ridge in non-hydrothermally influenced water in order to determine "background" water conditions.

Figure 1. (a) Regional map showing location of Endeavour Ridge. (b) Station locations (numbered circles) and bottom topography (map courtesy of C. Fox, NOAA) of the study region. See Table 1 for exact station locations. Heavy line marks the path of tow-yo.

Figure 1
Endeavour Ridge Topography

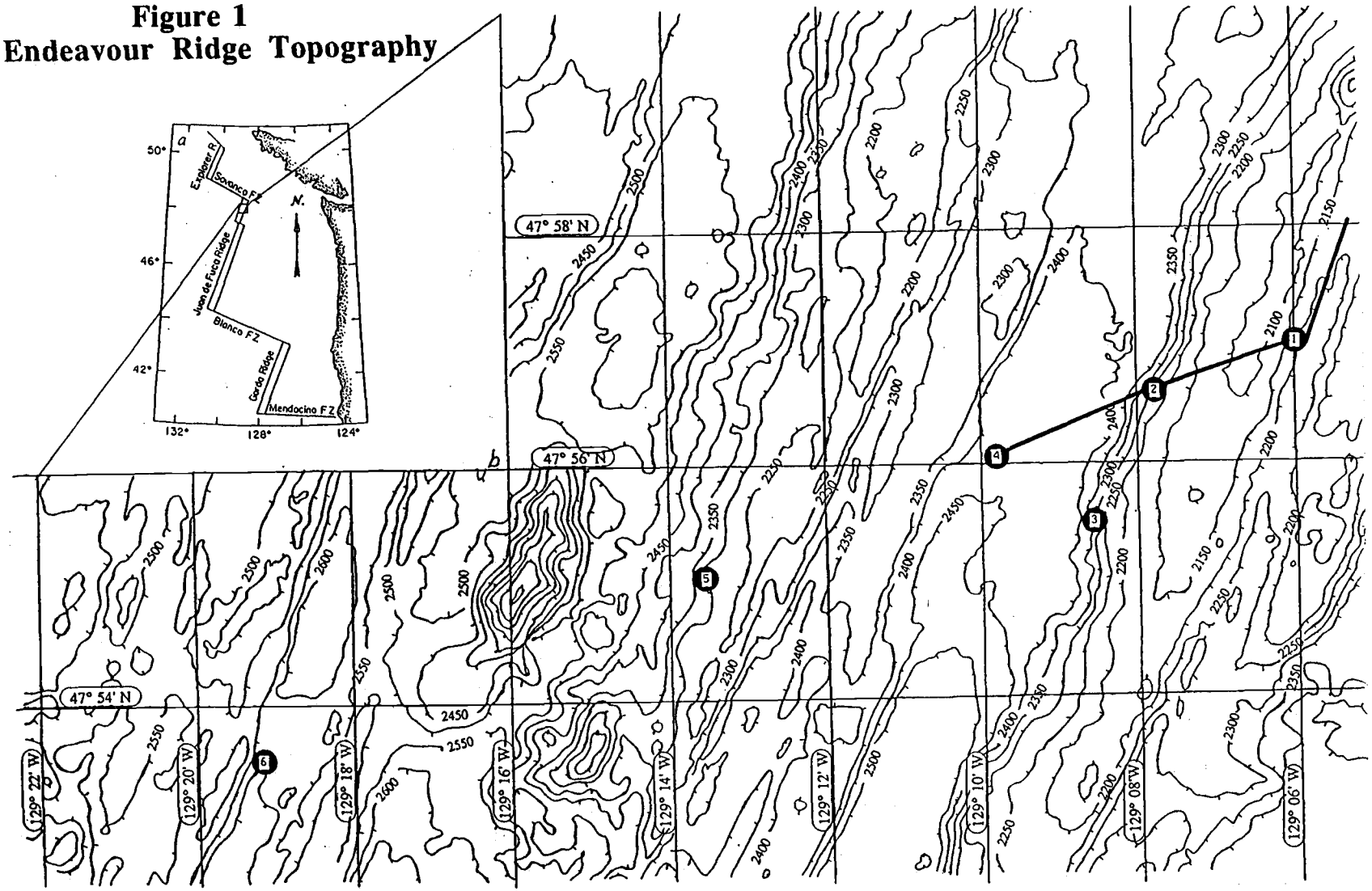

Table 1

Station Locations

Map Location	Station Type	Station No.	Latitude (°N)	Longitude (°W)
1	Vent Field	P2CTD1	47° 56.98	129° 06.04
1	Vent Field	P2CTD3	47° 56.97	129° 06.24
1	Vent Field	P2CTD12	47° 56.88	129° 05.90
1	Vent Field	P2CTD15	47° 56.88	129° 05.99
2	2 km	P2CTD9	47° 56.57	129° 07.60
3	4 km	P2CTD6	47° 55.50	129° 08.45
4	4 km	P2CTD4	47° 56.09	129° 09.57
5	10 km	P2CTD10	47° 55.10	129° 13.57
5	10 km	P2CTD11	47° 55.00	129° 13.56
6	17 km	P2CTD16	47° 53.53	129° 19.08
6	17 km	P2CTD18	47° 53.52	129° 19.18
NOT SHOWN	Background	P2CTD13	47° 57.57	128° 57.82

Samples were collected in acid-cleaned, 30-L PVC sample bottles (Go-Flo® and standard Niskin® bottles) mounted on an epoxy-coated, stainless steel rosette equipped with a Seabird® CTD and a Seatech® light transmissometer. The CTD/rosette was lowered through the hydrothermal plume to within a few meters of the seafloor. Based on the downcast profiles of light transmission and temperature anomalies, water column samples were collected on the upcast at depths which would best describe the plume's features. Drift in the temperature and conductivity measuring instruments, and light transmissometer were negligible over the 10 day cruise as demonstrated by stable water column values in non-hydrothermally influenced water at the vent stations occupied throughout the cruise.

Approximately 500-ml of water was drawn from the CTD/rosette bottles immediately after gas samples were drawn. Approximately 250-ml of each sample was immediately filtered through acid-cleaned, 0.4 μm pore diameter Nuclepore® polycarbonate filters. Afterwards, both the filtered and the unfiltered samples were acidified with subboiling-distilled, 6 N HCl to pH < 2, and stored. This technique yields an operational definition of "dissolved" as that which passes through the 0.4 μm pores of the filters. In this thesis, I shall refer to the unfiltered sample analyses as total concentrations, to the filtered samples as dissolved concentrations, and to the difference between the two as particle concentrations. Note that the dissolved iron samples do not actually represent reduced iron, or Fe(II). Studies have shown oxidized, iron particles as small as 1 to 20 nm in diameter (Campbell, et al., 1990), in the buoyant plume. Therefore, "dissolved iron" represents iron less than 0.4 μm in diameter.

III. Onshore Laboratory Procedures

The samples were returned to the lab and analyzed for both iron and manganese concentrations. Samples for manganese analysis were preconcentrated using an 8-Hydroxyquinoline solvent extraction technique (Klinkhammer, 1980; Landing and Bruland, 1987). The procedure is described in detail in Appendix B. The iron analysis used

an APDC (ammonium pyrrolidine dithiocarbamate) cobalt co-precipitation. After the preconcentration procedures the iron and manganese samples were analyzed by graphite furnace atomic absorption spectrophotometry (GFAAS) using a Perkin-Elmer 5000 instrument with the Zeeman effect background correction, an HGA-400 Heated Graphite Atomizer, and an AS-40 Autosampler. Overall precision of both techniques is estimated to be ±5%.

IV. CTD Data Processing

The background hydrocast, P2CTD13, made 10 km east of the ridge,was used to determine the background characteristics of the water in the Endeavour Ridge region in the absence of hydrothermal venting. The data from this hydrocast demonstrated a completely linear relationship between potential temperature (θ) and density referenced to the 2000 db level (σ_2) from 1600 meters to 2400 meters (Figure 2). I assume that in the absence of hydrothermal venting, this relationship would apply throughout our study region shown in Figure 1. This relationship was used to predict the "background" θ of other hydrocast stations based on the observed σ_2 profiles. The predicted θ was subtracted from the measured θ to obtain the excess temperature, or ΔT.

The vent field, 2 km, and 4 km stations seem to have the same water column characteristics as the background station. This is demonstrated by the calculation of $\Delta T = 0$ in non-plume water (above and below the plume). However, the 10 and 17 km stations have a different θ-σ_2 relationship than the background station in non-plume water (Figure 3). The actual difference between the ΔTs predicted for typical plume depths by the two relationships is about 3 times the standard deviation of 0.002 °C of the correlations. Although this amount of error is not significant at the vent field stations, it leads to a large error at the far-field stations. Because of this, using P2CTD13 as the background would result in the calculation of negative ΔTs above the plume at the 10 and 17-km stations (Figure 4). Since I depend on ΔT as a conservative tracer, I shifted the ΔT profile of the 10 and 17-km

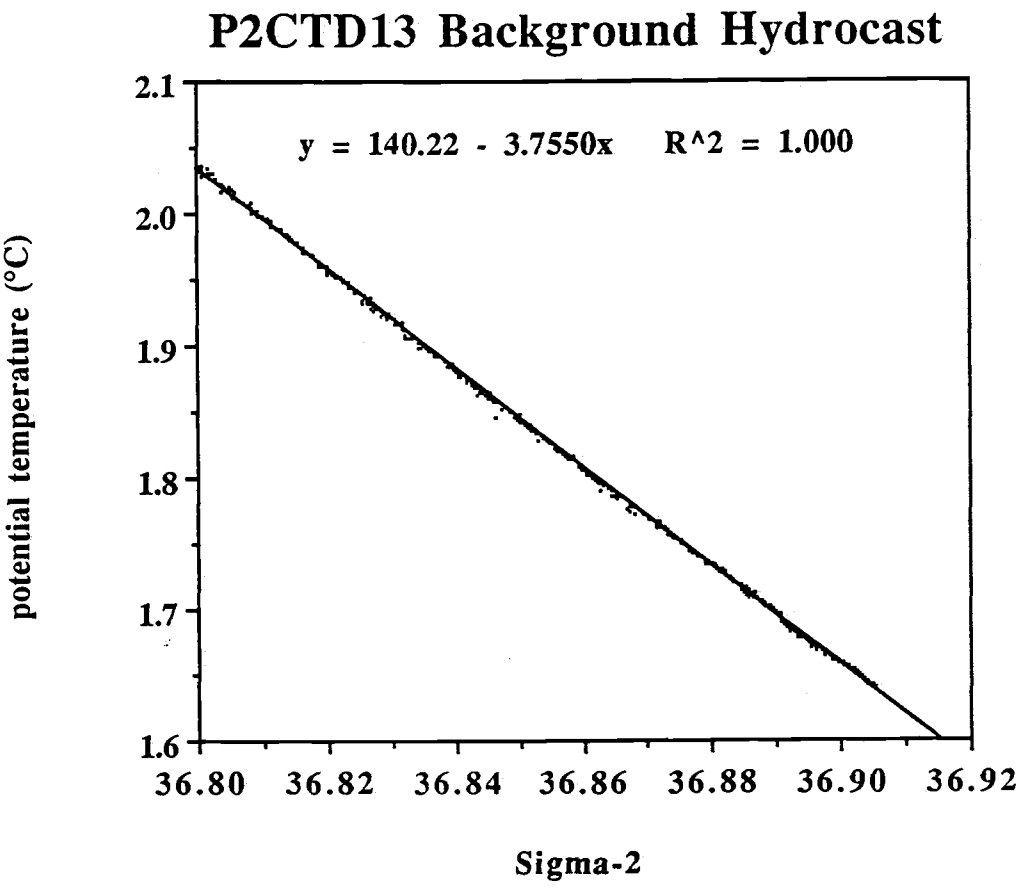

Figure 2. θ vs. σ_2 for the P2CTD13 "background" hydrocast. The linear correlation fit given is used to predict the "background" potential temperature.

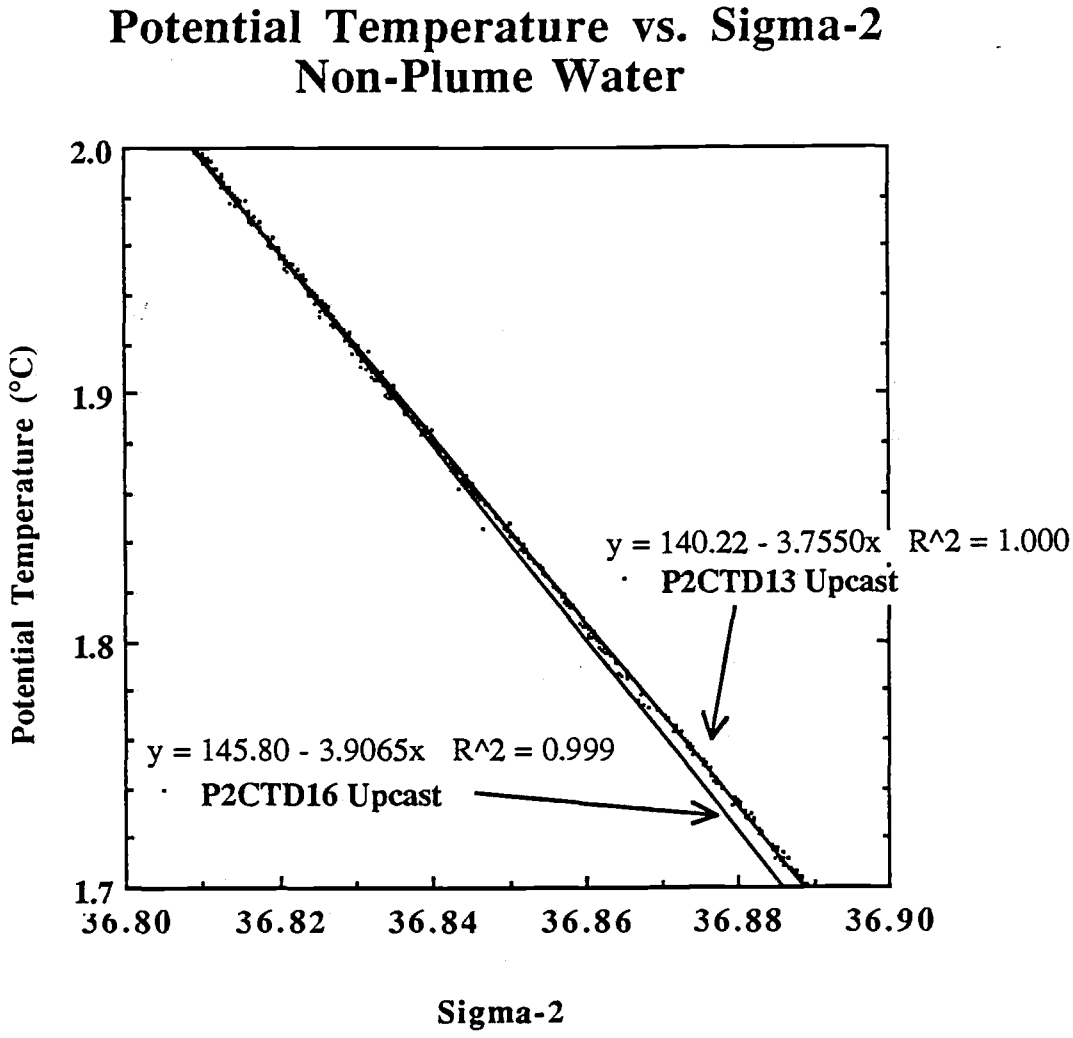

Figure 3. θ vs. σ_2 for the P2CTD13 "background" hydrocast vs. that for the non-plume portion of the P2CTD16 17-km hydrocast. The P2CTD16 17-km hydrocast shows a larger slope than the "background" hydrocast.

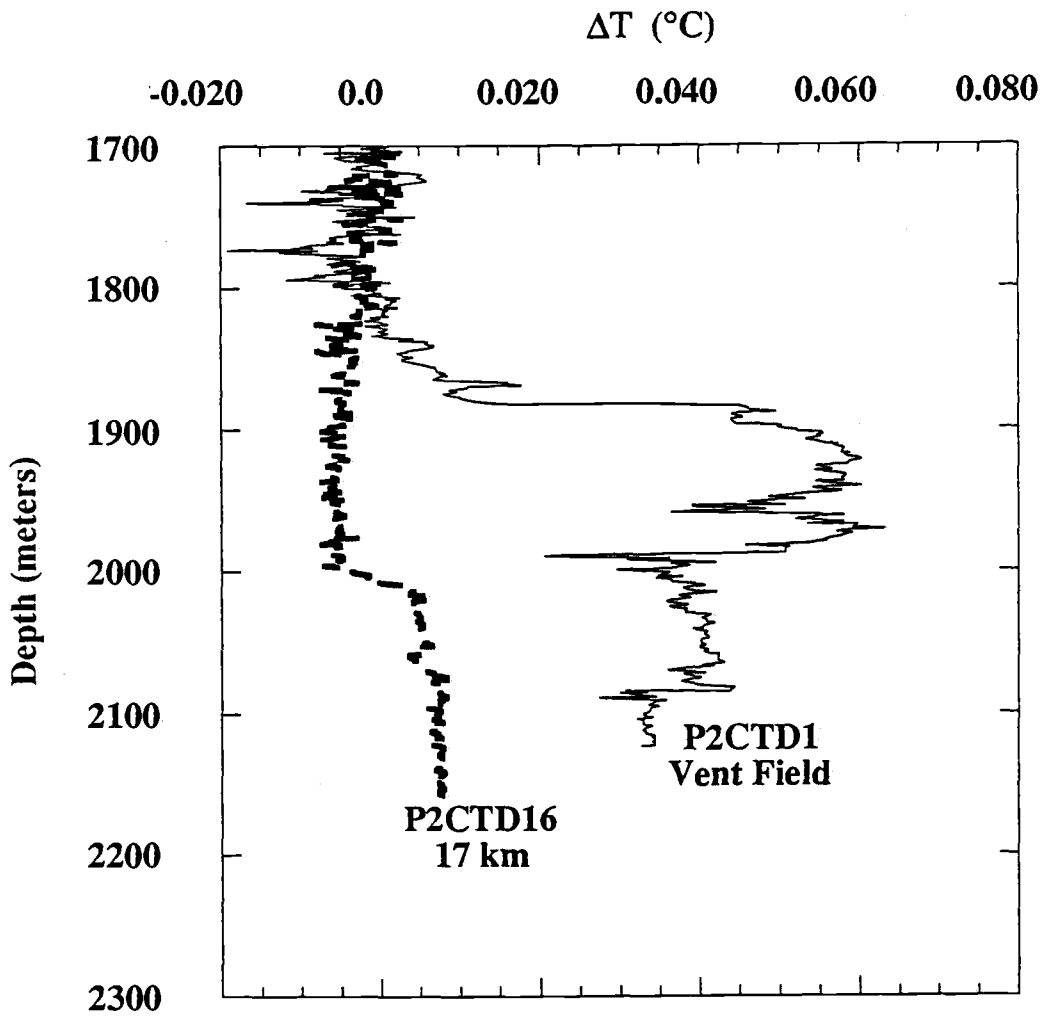

Figure 4. ΔT profiles for the P2CTD1 vent field hydrocast vs. that for the P2CTD16 17-km hydrocast using the P2CTD13 "background" hydrocast to predict ΔT. Note the approximately vertical slope centered at ΔT= 0 for P2CTD1 vs. that for the P2CTD16 17-km hydrocast.

stations to make $\Delta T = 0$ at the top of the plume. However, the water column characteristics continue to diverge below this point in the plume. Using the 17-km stations' non-plume water to get a background θ-σ_2 relationship would result in ΔTs approximately 50% larger than those used here.

The reason for the different background water column characteristics is unknown. Either the plume at the far-field stations has been diluted by different water masses, or the background station has been hydrothermally influenced. As mentioned previously, a linear relationship between θ and σ_2 at the background station indicates no significant hydrothermal influence. Also, these differing water column characteristics extend above normal plume depths. I feel that these differences are hydrographic in nature, and result from the various flow regimes in and around the ridge crest.

Some investigators have used a θ-σ_θ (referenced to zero db) relationship to calculate ΔT (Baker, et al., 1989; Baker and Massoth, 1986; Baker and Massoth, 1987; Baker, et al., 1990). Using a θ-σ_θ relationship, I would calculate a ΔT approximately 25% larger than those from a θ-σ_2 relationship (Figure 5). I have also used a θ_2-σ_2 relationship to calculate ΔT, and found those to be equal to those calculated by a θ-σ_2 relationship. Either density reference level could be used to calculate the dilution of ΔT in the neutrally buoyant plume, as long as consistency is maintained. However, the choice of reference level will affect the comparison of metal/ΔT ratios in the plume to those in the vents, as described below.

Light anomalies (ΔL) are reported in units of m^{-1}. Light % transmission values are converted into m^{-1} by the equation:

$$-\ln (\%\ \text{Transmission}/100) \div 0.25\ \text{meters} = R\ (m^{-1}) \qquad (1)$$

where R is an index of the light absorbance. Light anomalies were calculated by subtracting the above-plume "clear water" values from those values measured in the plume:

$$\Delta L = R_{plume} - R_{above\ plume} \qquad (2)$$

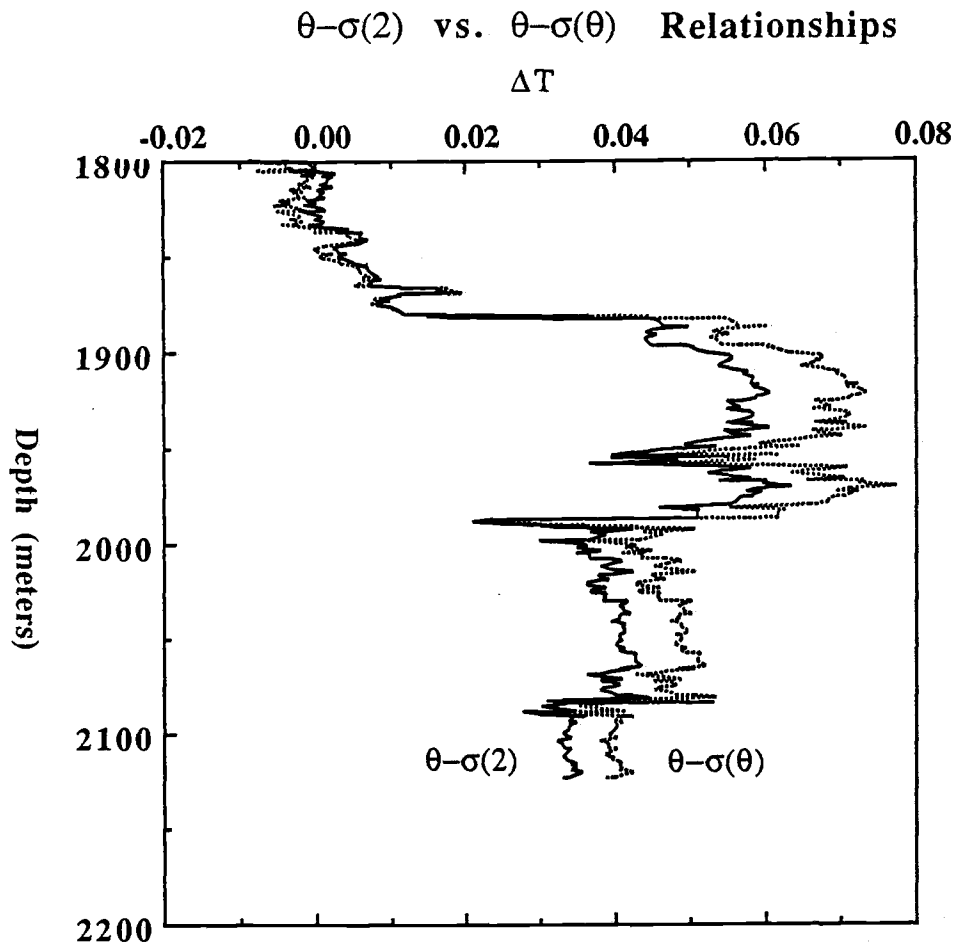

Figure 5. ΔT profiles for the P2CTD1 vent field hydrocast predicted by using a θ-σ_2 relationship (solid line) vs. a θ-σ_θ relationship (dotted line). The integrated ΔT using the θ-σ_θ relationship predicts a 25% larger ΔT.

The iron and manganese concentrations, the ΔT, and the ΔL values were integrated over the depth ranges of the neutrally buoyant plume. In order to estimate the rate of removal of a transient tracer from the plume, a non-reactive or conservative tracer is needed to estimate the degree of dilution of the plume. Frequently, ^3He is used since any decrease in ^3He content is due to dilution of the vent water by entrained seawater with low ^3He content. Since, the ^3He samples from the 10 and 17-km stations are not available, I used excess temperature (ΔT) as a conservative tracer. The integrated iron and manganese concentrations were divided by the integrated ΔT values. In this approach, non-conservative behavior of a hydrothermal tracer is indicated by decreasing tracer/ΔT ratio at increasing distance from the vent field.

RESULTS AND DISCUSSION

I. Results

The ΔT, ΔL, and both dissolved and total iron and manganese profiles are shown in Appendix B. The profiles are presented in the order of increasing distance from the vent field. As examples, the profiles for the P2CTD1 vent field station and the P2CTD16 17-km station are shown as Figures 6 and 7, respectively. The complexity of the vent field plume structure is illustrated best by the ΔT and ΔL profiles in Figure 6A. All hydrocasts that were taken directly over the vent field had multiple maxima and density inversions. Compare this to the rather simple structure of the plume in Figure 7A, after it has been advected 17 km. The overlap of the dissolved and total manganese profiles in Figure 6B shows that essentially all of the manganese is dissolved at the vent field. In Figure 7B, I see that approximately 30% of the manganese at the 17-km station is associated with particles. Figure 6C, the dissolved and total iron profiles, indicates that approximately 50% of the iron on suspended particles over the vent field is less than 0.4 μm in diameter. Figure 7C shows some complexity in the iron profiles, due to decreased precision in the iron analysis at low concentrations. However, only about 30% of the iron is less than 0.4 μm in diameter at the 17-km station.

Not all hydrocasts were analyzed for all constituents. For example, no trace metal samples were taken for the P2CTD4 4-km hydrocast. Therefore, only the temperature and light anomaly data are presented. The light transmissometer failed during the P2CTD6 hydrocast and therefore is not presented. For clarity, the graphs are shown in the same position on each page.

The data from each hydrocast was integrated over the depth range of the neutrally buoyant plume using the commercial software program Kaleidagraph® on a Macintosh IIci computer. The integrated values of these parameters are given in Table 2.

Figure 6. P2CTD1 profiles: (A) ΔL (m^{-1}) and ΔT (°C), (B) total and dissolved Mn (nmoles/kg), (C) total and dissolved Fe (nmoles/kg).

Figure 6 - P2CTD1 (Vent Field) Profiles

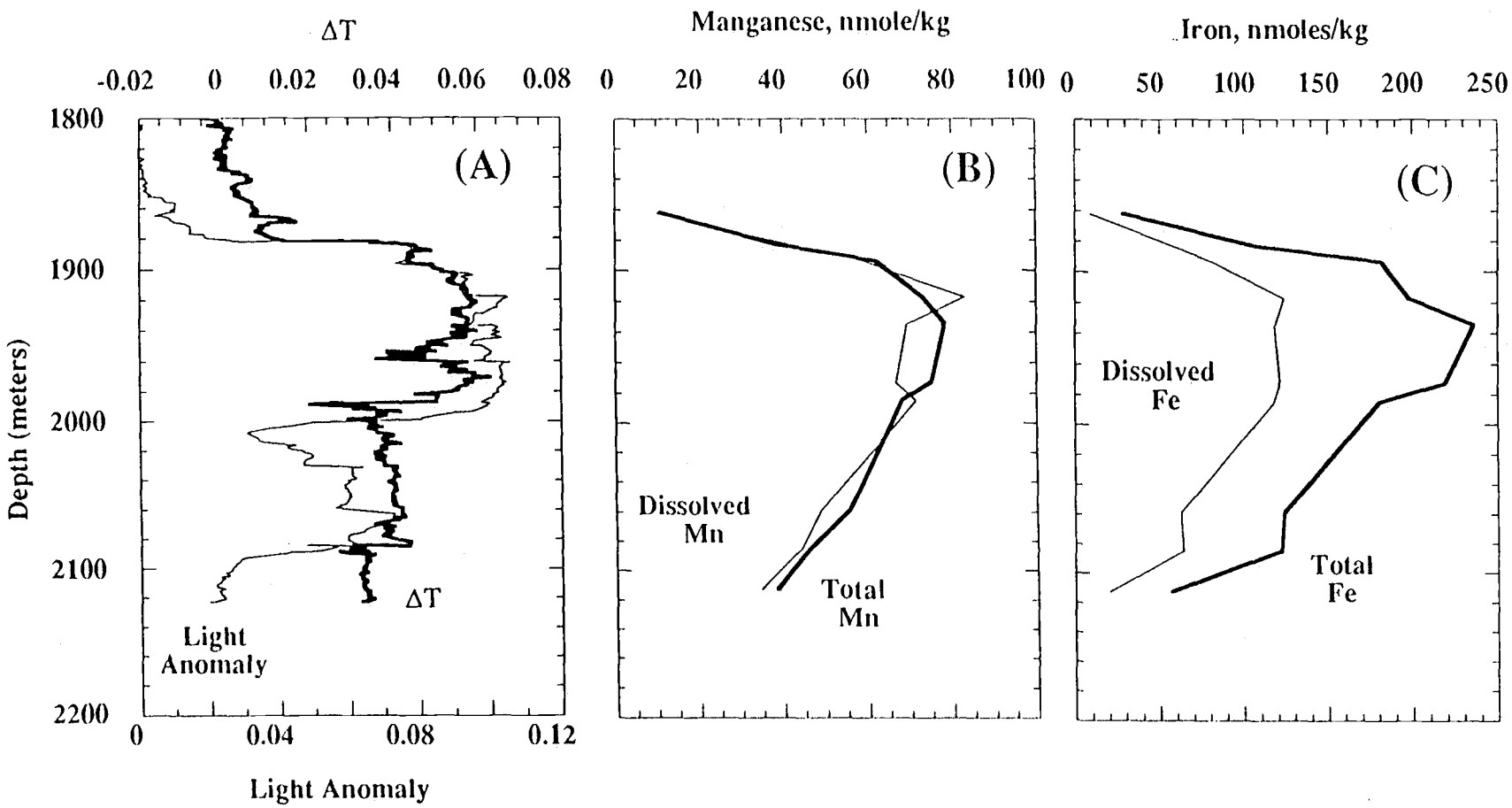

Figure 7. P2CTD16 profiles: (A) ΔL (m^{-1}) and ΔT (°C), (B) total and dissolved Mn (nmoles/kg), (C) total and dissolved Fe (nmoles/kg).

Figure 7 - P2CTD16 (17 km) Profiles

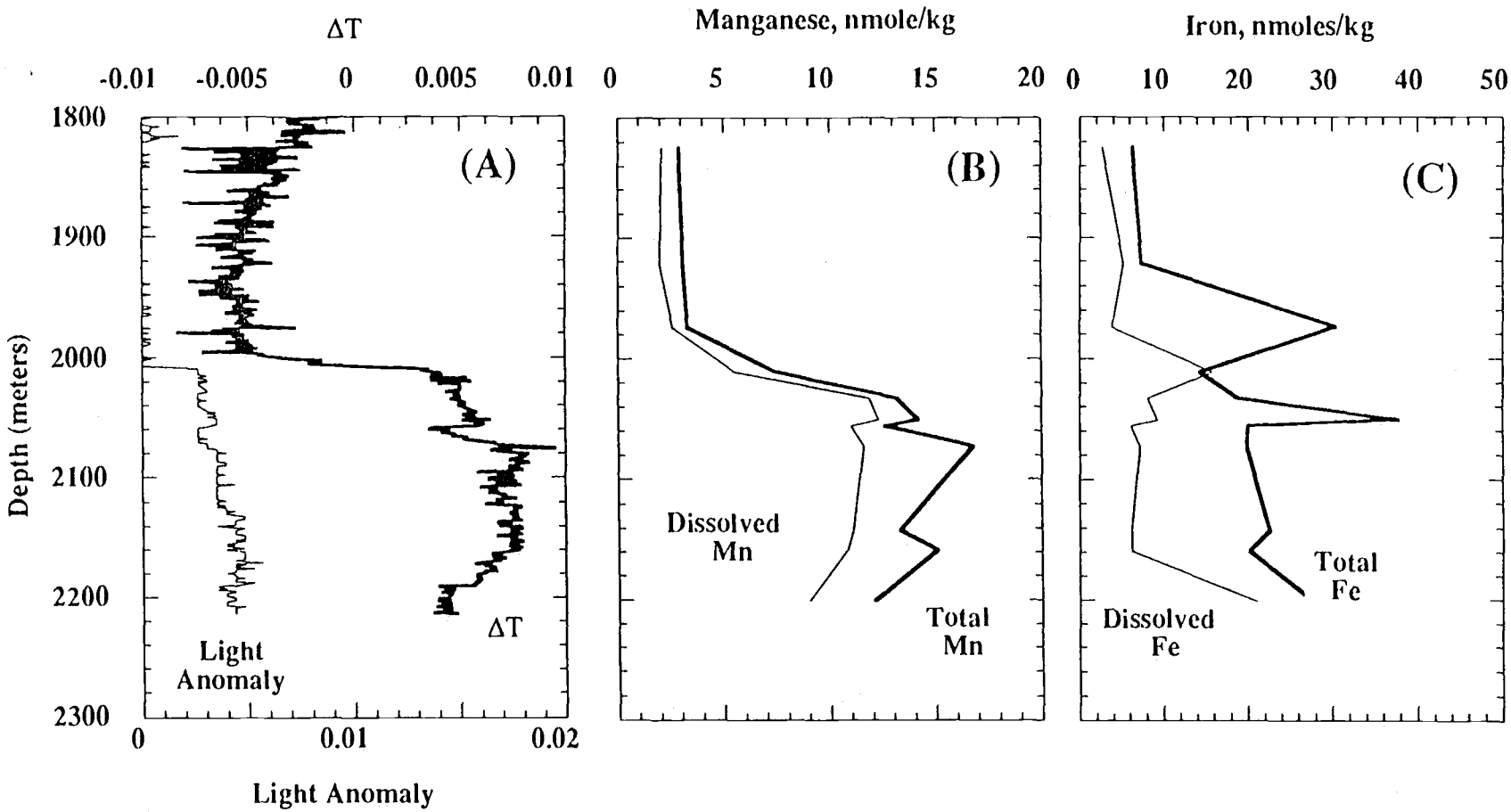

Table 2
Integrated Parameters

Parameter	P2CTD1	P2CTD3	P2CTD12	P2CTD15	P2CTD9
Distance from vent field, km	0	0	0	0	2
Integration depth, m	1862-2113	1800-2156	1800-2147	1878-2146	1844-2135
$\Sigma \Delta L$ (Light anomaly), $m \cdot m^{-1}$	16.994	9.312	6.322	7.525	6.735
$\Sigma \Delta T$ (Temperatureanomaly), $m \cdot °C$	10.494	9.736	10.206	9.179	10.204
Σ Total [Mn], m·nmoles/kg	14831	15233	16546	14079	15769
Σ Filtered [Mn], m·nmoles/kg	14284	15068	-	14282	15994
Σ Total [Fe], m·nmoles/kg	39213	35108	-	-	28471
Σ Filtered [Fe], m·nmoles/kg	21460	15879	-	-	7062
$\Sigma \Delta L / S \Delta T$, $m^{-1}/°C$	1.62	0.96	0.62	0.82	0.66
Σ Total [Mn]/$\Sigma \Delta T$, nmoles Mn/kg/°C	1413	1565	1621	1534	1545
Σ Filtered [Mn]/$\Sigma \Delta T$, nmoles Mn/kg/°C	1361	1548	-	1556	1567
Σ Total [Fe]/$\Sigma \Delta T$, nmoles Fe/kg/°C	3737	3606	-	-	2790
Σ Filtered [Fe]/$\Sigma \Delta T$, nmoles Fe/kg/°C	2045	1631	-	-	692
Σ Part. [Fe]/$\Sigma \Delta T$, nmoles Fe/kg/°C	1692	1975	-	-	2098
Σ Total [Fe]/Σ Total [Mn]	2.64	2.30	-	-	1.81

Table 2 (continued)
Integrated Parameters

Parameter	P2CTD6	P2CTD10	P2CTD11	P2CTD16	P2CTD18
Distance from vent field, km	4	10	10	17	17
Integration depth, m	1865-2321	1829-2171	1912-2191	1900-2200	1950-2365
$\Sigma \Delta L$ (Light anomaly), $m \cdot m^{-1}$	-	1.882	1.82	0.759	1.536
$\Sigma \Delta T$ (Temperatureanomaly), $m \cdot °C$	6.941	5.061	5.579	2.81	3.357
Σ Total [Mn], m·nmoles/kg	11750	7344	6629	2879	4282
Σ Filtered [Mn], m·nmoles/kg	9838	6800	5802	2226	3000
Σ Total [Fe], m·nmoles/kg	17388	-	9554	4626	-
Σ Filtered [Fe], m·nmoles/kg	6262	-	3305	1849	-
$\Sigma \Delta L/S \Delta T$, $m^{-1}/°C$	-	0.37	0.33	0.27	0.46
Σ Total [Mn]/$\Sigma \Delta T$, nmoles Mn/kg/°C	1693	1451	1188	1025	1276
Σ Filtered [Mn]/$\Sigma \Delta T$, nmoles Mn/kg/°C	1417	1344	1040	792	894
Σ Total [Fe]/$\Sigma \Delta T$, nmoles Fe/kg/°C	2505	-	1712	1646	-
Σ Filtered [Fe]/$\Sigma \Delta T$, nmoles Fe/kg/°C	902	-	592	658	-
Σ Part. [Fe]/$\Sigma \Delta T$, nmoles Fe/kg/°C	1602	-	1120	988	-
Σ Total [Fe]/Σ Total [Mn]	1.48	-	1.44	1.61	-

II. Evolution of the Neutrally Buoyant Plume

Figure 8 is a ΔT section extending from the vent field WSW to the 17-km stations. In Figure 1 and Table 1, it can be seen that 2 stations were occupied 4 km from the vent field. One station, P2CTD4, was aligned with the other stations and was used in the construction of the ΔT section. The other station, P2CTD6, was located south of P2CTD4. The ΔT profile for P2CTD4 (Figure 25) shows two maxima, similar to the profiles at the 10-km stations (Figures 27 and 28). However, at the 17-km stations (Figures 29 and 30), the upper maxima has disappeared. The origin of the upper maxima could be the integration of different plumes or possibly a large eddy caused by the advection of the plume over the western axial valley summit.

The water of the upper maxima appears to be moving in a different direction than the lower water. Figure 9 is a section of σ_2 for the same stations in Figure 8. It can be seen that the isopycnals are spread apart at the 2-km stations, with the $\sigma_2 = 36.855$ isopycnal remaining nearly level at approximately 1900 meters. Geostrophic velocities change vertically if density changes horizontally. Assuming this horizontal σ_2 surface (~1900 meters) as a level of zero motion, geostrophic flow below 1900 meters is predicted to be southward from the vent field to 2 km and northward from 2 km to 17 km. Geostrophic flow above 1900 meters is predicted to be northward from the vent field to 2 km and southward from 2 to 17 km. The geostrophic velocities would be imposed on any regional velocities and directions. The prediction of currents that parallel the ridge matches those directions found by others (Cannon, et al., 1990; Cannon and Pahinski, 1990). The main observation is that the plume above 1900 meters appears to be advecting more southward, as it moves away from the ridge, and is thus absent in the 17-km stations' profiles.

These data suggest significant complexity in the near-ridge flows which could be either topographically induced or dynamically generated by the vent buoyancy flux. However, once away from the ridge crest, the plume was being advected in a southwestern direction (determined by tow-yo hydrocasts).

Figure 8. ΔT section extending from vent field to 17-km station. Bottom topography taken from Figure 1. Vertical dashed lines indicate station locations. Note spreading of lines of constant ΔT at 2-km station.

Figure 8 - ΔT Section

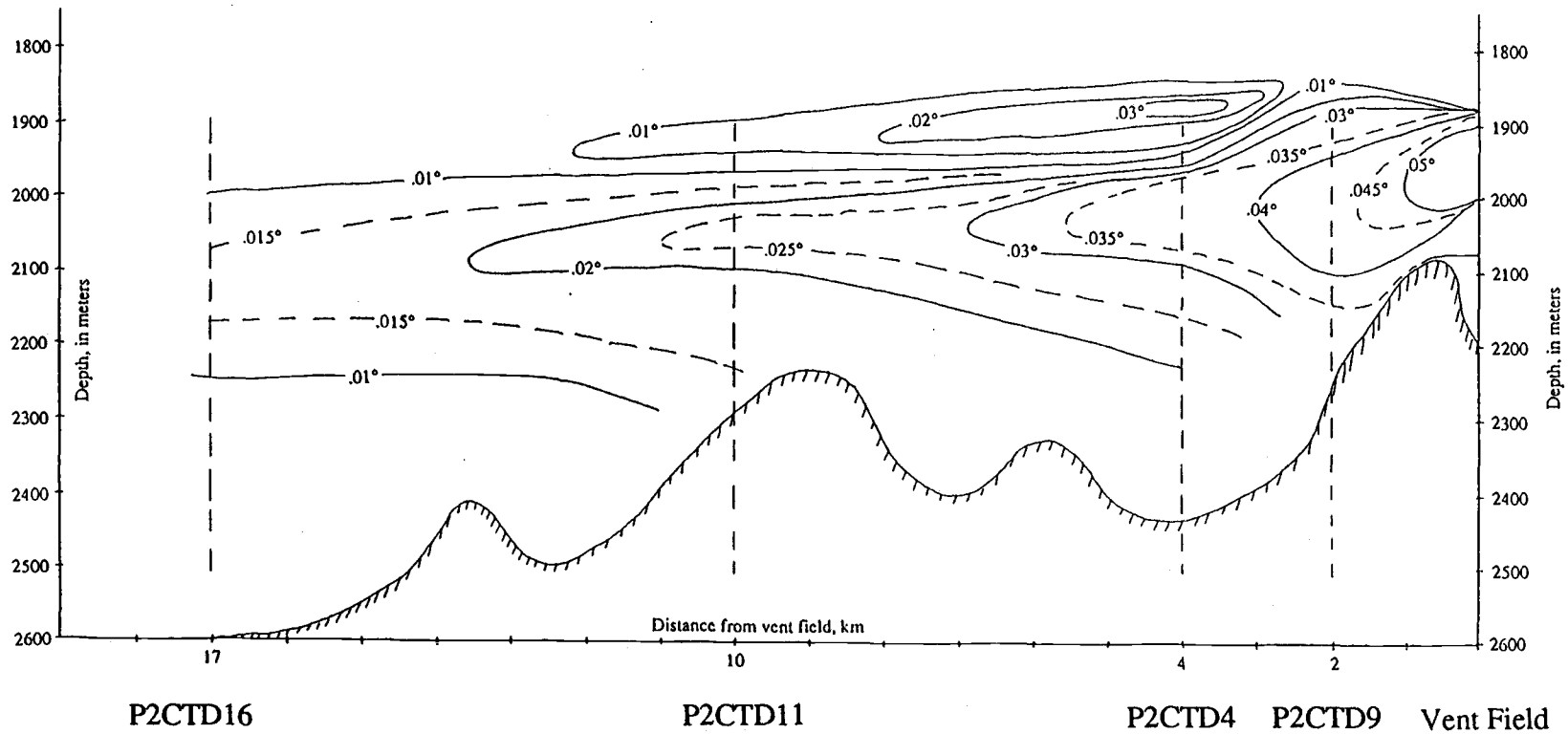

Figure 9. σ_2 section extending from vent field to 17-km station similar to ΔT section of Figure 8. Bottom topography taken from Figure 1. Vertical dashed lines indicate station locations. Note spreading of isopycnals at 2-km station.

Figure 9 - σ_2 Section

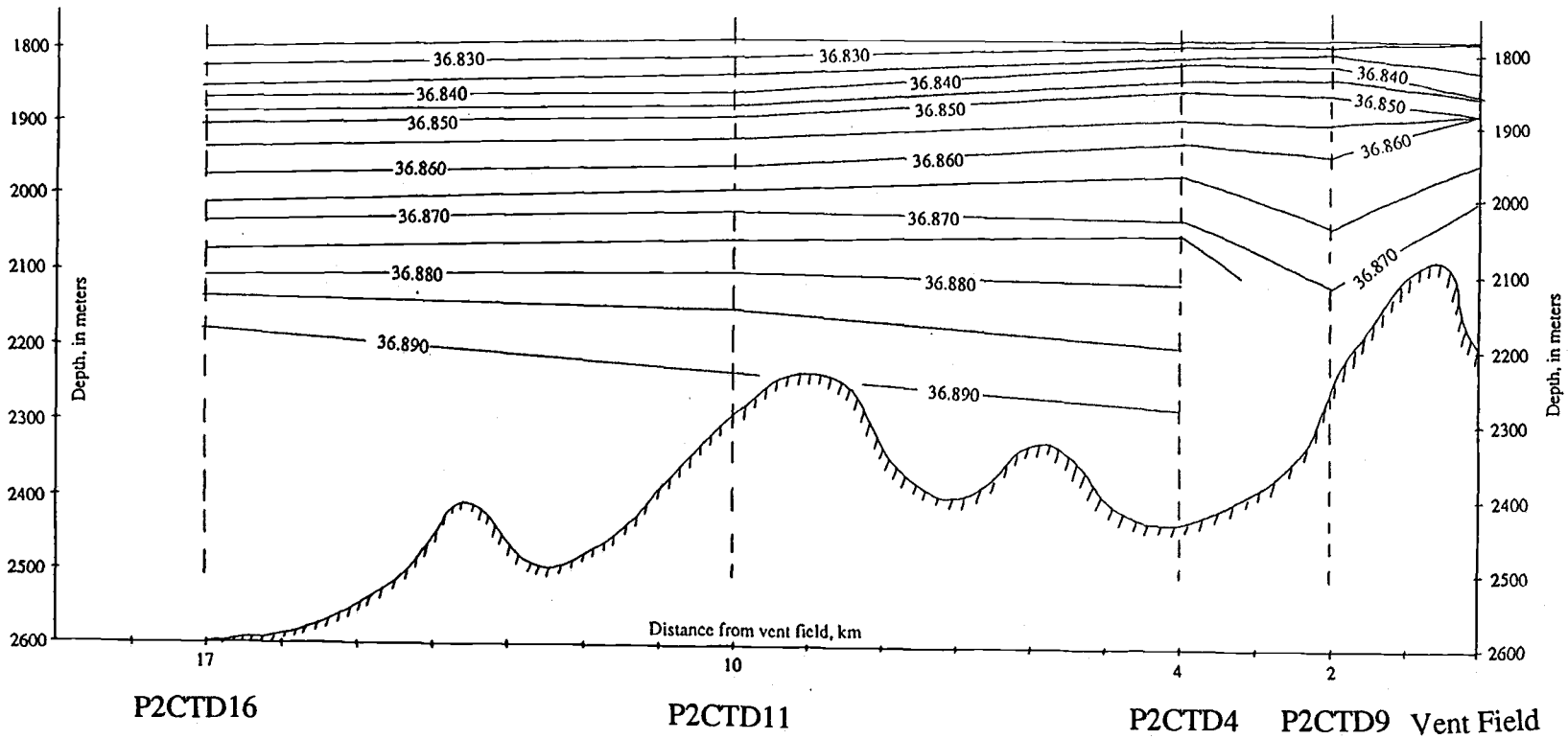

III. Manganese, Iron, and Heat at the Vent Field

Oceanographers know that the iron and manganese from hydrothermal vents eventually finds its way into the sediments around mid-ocean ridges. However, we don't know the mechanisms by which this is accomplished or the rates of these mechanisms. Many investigators are trying to determine if manganese is oxidized and scavenged in the particle-rich environment during the approximately one hour time-of-rise of the buoyant plume. Manganese concentrations have been normalized to conservative tracers such as ^{3}He concentration (Kadko, et al., 1990; Lupton, 1990; Lupton, et al., 1980; Weiss, 1977), silicate concentration (Elderfield, et al., 1990; Klinkhammer, et al., 1986), and heat content (Baker and Massoth, 1986; Klinkhammer, et al., 1986). Kadko, et al., 1990 found higher Mn/heat ratios in the neutrally buoyant plume than in the vents at Endeavour Ridge. Lupton, 1990; Lupton, et al., 1980; Baker and Massoth, 1986; Elderfield, et al., 1990; and Klinkhammer, et al., 1986 found lower Mn/tracer ratios in the plumes than in the vents at various vent fields on the East Pacific Rise and on the Mid-Atlantic Ridge. A possible problem with a direct comparison to the high-temperature end-member is the assumption that the high-temperature vents are the main contributors to the neutrally buoyant plume. Recent studies on the Juan de Fuca Ridge show evidence that low-temperature venting may be responsible for as much as an order of magnitude more heat flux than discrete high-temperature vents (Rona and Trivett, 1990; Schultz, et al., 1990). Observations of low-temperature venting are ubiquitous at these vent fields. The variation in the extraction efficiency of the various conservative tracers at lower temperatures is not well-constrained, and may be the reason for the varying manganese/tracer ratios observed by others in the plumes vs. those in the high-temperature vents.

Investigators have also examined particles from the buoyant plumes and neutrally-bouyant plumes near the vent fields for evidence of particulate manganese. Little evidence was found for the scavenging of manganese by particles (Baker and Massoth, 1986; Campbell, et al., 1990; Campbell, et al., 1988; Mottl and McConachy, 1990; Trefry, et

al., 1985; Trocine and Trefry, 1988). Particulate manganese was found near the vent field only in the Guaymas Basin. There the hydrothermal waters are confined to a basin for a period of time, and the conclusion is that a metal-oxidizing bacterial population is responsible for the removal of manganese on a time scale of days.

At Endeavour Ridge, I will relate the manganese, the iron, and the heat content (represented by the excess temperature, or ΔT) of the plume to that in the vents. The difficulties in making such a comparison have been pointed out by many researchers (Elderfield, et al., 1990; Kadko, et al., 1990; Lupton, 1990; Lupton, et al., 1989; McDuff, 1988; Rosenberg, et al., 1988; Speer, 1988; Speer and Rona, 1989). The temperature and salinity characteristics of the vent water affect the temperature and salinity anomalies of the plume. In order to make meaningful comparisons, plume theory and modeling have to be used. A small sampling of the literature pertinent to oceanic hydrothermal plumes is presented in the reference list (Campbell, et al., 1984; Cann and Strens, 1989; List, 1982; Little, et al., 1987; McDougall, 1990; McDuff, 1988; Middleton, 1979; Middleton, 1986; Middleton and Thomson, 1986; Morton, 1959; Morton and Middleton, 1973; Morton, et al., 1956; Norton, 1984; Rouse, et al., 1952; Speer, 1988; Speer and Rona, 1989; Turner, 1969; Turner and Campbell, 1987; Turner and Gustafson, 1978). Many of the plume models use background temperature and salinity profiles and assume a vent temperature and salinity. However, vent waters are different in that they do not obey Marcet's Principle, which states that the salts in seawater are present in a fixed ratio. Pure high-temperature hydrothermal vent waters have no magnesium or sulfate, and can be enriched or depleted in chloride, sodium, calcium, and potassium relative to seawater. While a salinity for vent waters could be calculated, it would not be simply related to the salinity of the ambient seawater (determined by conductivity measurement on standard seawater). Rather than try to resolve this issue, I have assumed that chlorinity of the vent water multiplied by 1.806555 equals the salinity for the density calculations below. It has been suggested that a smaller proportionality constant would be appropriate for vent water salinity calculation [D. Butterfield, pers. comm.].

I have used the model of R. E. McDuff (McDuff, 1988) to calculate the metal/ΔT ratio of a plume that would be derived from the Endeavour Ridge vents. The manganese concentration in the high temperature vents at Endeavour Ridge ranges from approximately 200 μM at one vent in the northeast section of the vent field to 300 μM at three vents in the approximate center of the vent field [D. Butterfield, pers. comm.]. The central vents are estimated to contribute approximately 80% of the high-temperature flow from the Endeavour Ridge vent field [R. E. McDuff, pers. comm.]. The chlorinities of these high temperature fluids vary from approximately 47% to 94% of seawater. After correction for the effects of the properties of the vent fluid and the entrained water on ΔT at extreme dilutions (Baker, et al., 1990; McDuff, 1988), the Mn/ΔT ratio of a conservative plume derived from these vents is estimated to range from ~850 nmole Mn/kg/°C in the northeast vent to ~1300 nmole Mn/kg/°C at the three central vents. The effect of a lower proportionality constant for salinity calculation would be an increase in the calculated Mn/ΔT ratios of the vents. For example, a proportionality constant of 1.2 would result in a Mn/ΔT ratio for the three central vents of ~1500 nmole Mn/kg/°C.

Figure 10 is a comparison of the measured total manganese concentration and the measured excess temperature for all samples taken during the Plume2 cruise. A linear regression yields a line with a slope of approximately 1400 (±10%) nmole Mn/kg/°C. Another way of relating the two parameters is to divide the integrated manganese concentration by the integrated excess temperature to calculate a Mn/ΔT ratio for each station. These values were given in Table 2, along with all of the other integrated parameters. The average total Mn/ΔT of the four vent field stations is approximately 1500 (±6%) nmole Mn/kg/°C, which is equivalent to the linear regression estimate. Within wide limits, the agreement between the Mn/ΔT ratio of the central vents (1300 nmoles Mn/kg/°C) and that in the neutrally buoyant plume (1400 to 1500 ±10% nmoles Mn/kg/°C) supports the view that little manganese is lost during the buoyant rise of the plume.

The Fe/ΔT ratios of the vents range from ~2200 nmoles Fe/kg/°C at the northeast vent to ~4400 nmoles Fe/kg/°C at the three central vents.

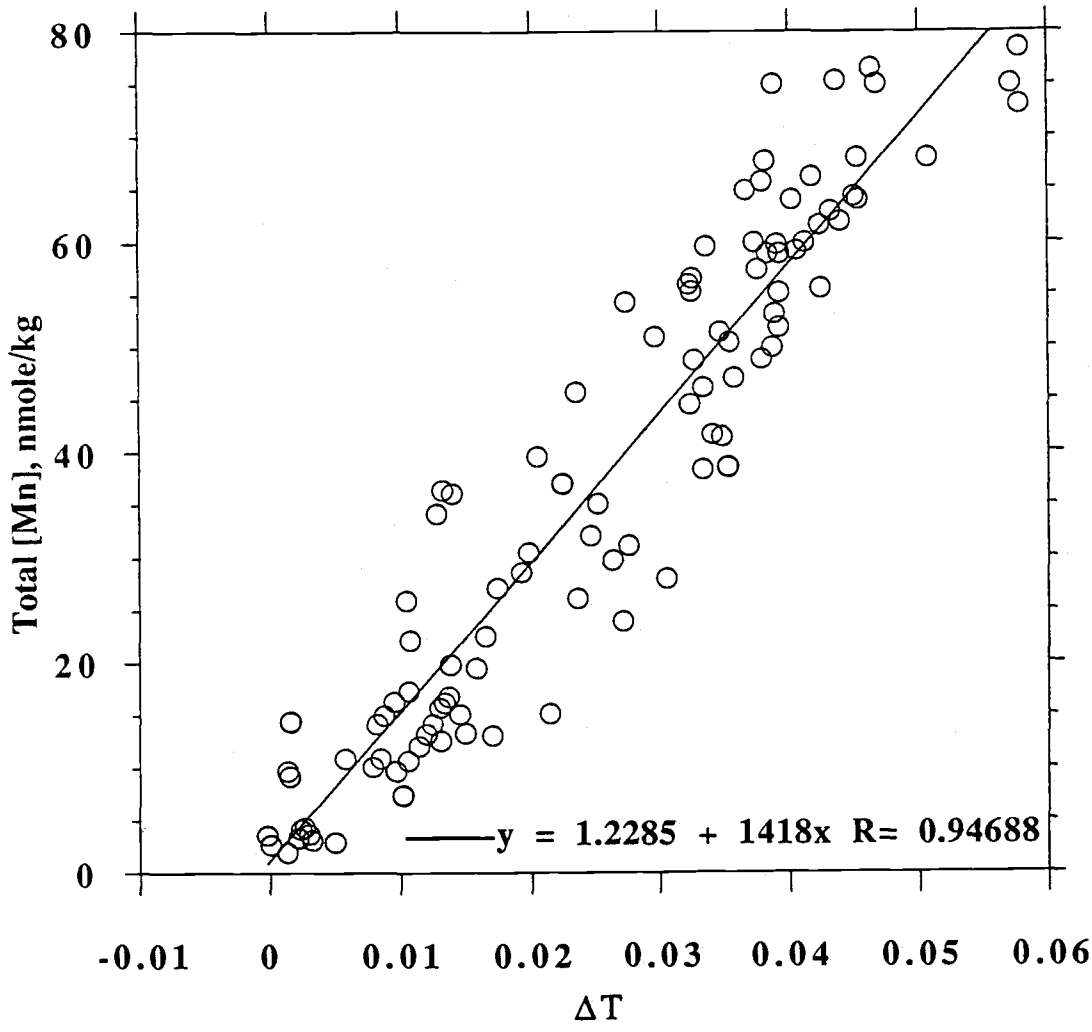

Figure 10. Total [Mn] vs. ΔT for all samples analyzed. A linear regression is drawn through the data and the fit is given with R = 0.95.

The Fe/ΔT ratio of the neutrally buoyant plume over the vent field is ~3700 nmoles Fe/kg/°C. Either ~15% of the iron is lost during the plume's buoyant rise, or there is a source with a low Fe/ΔT ratio contributing to the neutrally buoyant plume. Either explanation is possible and, in fact, both may be correct.

Figure 11 shows the manganese, iron, and ΔT profiles for the four vent field stations occupied during the cruise. It can be seen that manganese, iron, and ΔT remain elevated all the way down to the axial valley floor. Diffuse warm springs have been suggested as a source of these elevated temperatures in the lower 100 meters of the water column at Endeavour Ridge (Baker and Massoth, 1987). Several investigators have noted pervasive, low-temperature venting at Endeavour Ridge (Hammond, et al., 1984; Schultz, 1989; Tivey and Delaney, 1986). Although low-temperature venting will not have the buoyancy flux needed to rise to the heights of the neutrally buoyant plumes, it can influence the manganese concentration, heat content, and other properties of the local bottom water that is entrained in the buoyant plumes. Clearly, the entrained water is not free of Mn, Fe, and heat as would be assumed by models that used "zero" for these quantities. This water makes up a large fraction of the plume water, which is discussed below. The final composition of the neutrally buoyant plume can be as sensitive to the properties of the entrained water as it is to the properties of the primary vents.

Quantifying the contribution of low-temperature venting to the neutrally buoyant plume is not straightforward. One important observation is that the near-bottom water has approximately the same Mn/ΔT ratio as the vents. This seems reasonable if the low-temperature venting results from subsurface mixing of high-temperature fluids and ambient seawater without removal of manganese. However, the similarity of the Mn/ΔT ratios in the plume, the near-bottom water, and the vents makes it impossible to quantify individual contributions using these ratios. However, the Fe/ΔT ratio varies from the vents (4400 nmoles/kg/°C) to the plume (3700 nmoles/kg/°C) to the bottom water (1700 nmoles/kg/°C). A plume made of approximately 25% bottom water and 75% water that was affected primarily by high-temperature

Figure 11. Profiles of [Mn], [Fe], and ΔT for the four vent field stations occupied during the cruise. Note the x-axis scale changes from P2CTD1, P2CTD3 to P2CTD12, P2CTD15. Also, note that the anomalies remain elevated all the way down to the axial valley floor.

Figure 11 - Vent Field Hydrocast Profiles

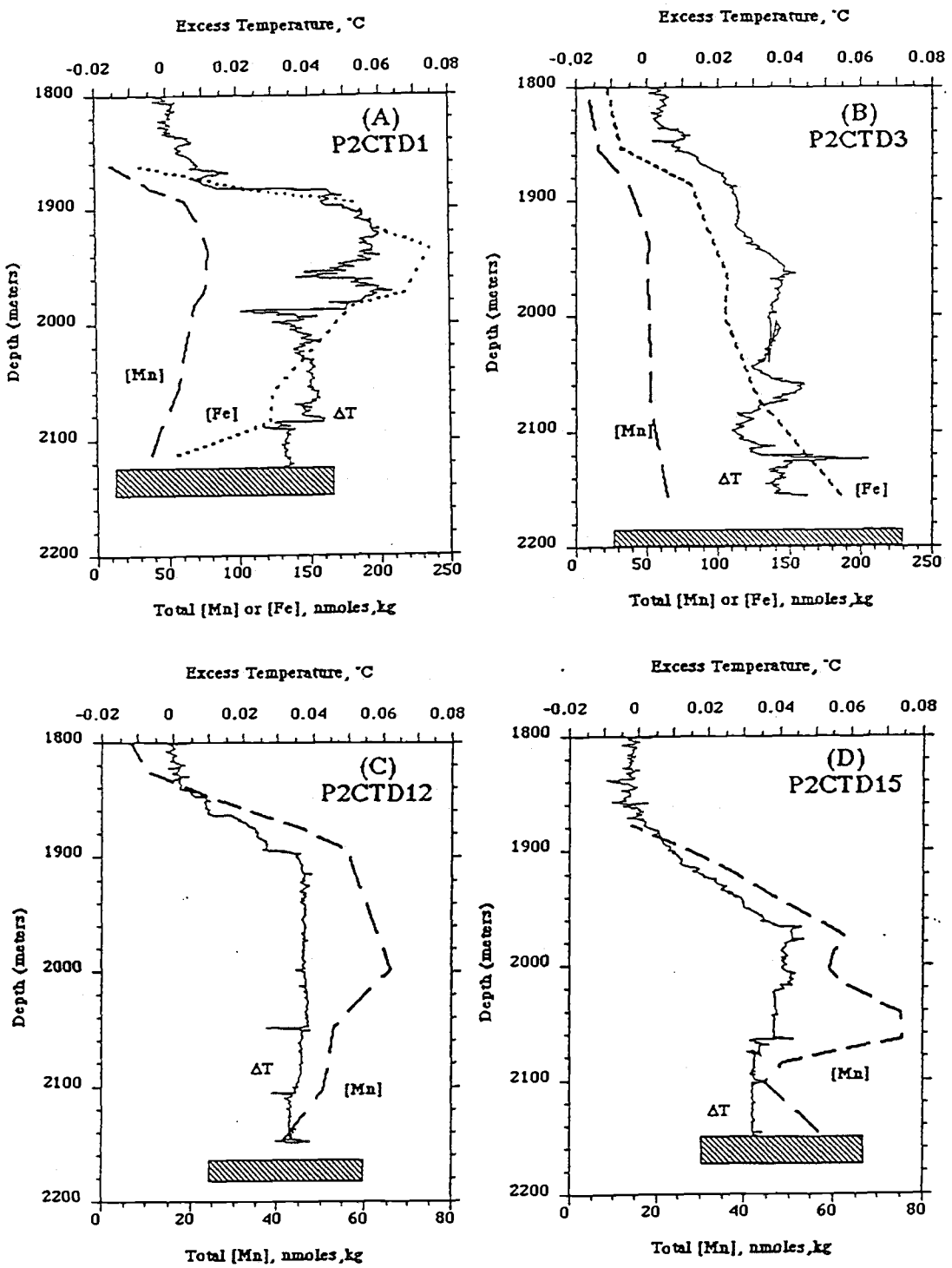

venting would give the neutrally buoyant plume's Fe/ΔT ratio. However, the bottom water's Fe/ΔT ratio is not well-constrained, and this type of analysis should be used guardedly.

Another possibility is to use the composition of the neutrally buoyant plume, which is estimated to be ~70% entrained water, ~30% ambient water, and ~0.01% vent fluid (Lupton, et al., 1985). Entrained water is water that has been advected from deeper in the water column. Ambient water is water that is normally found at a particular depth. These values were calculated based on salinity differences between the plume and ambient water and the assumption that all of the entrained water came from the depth of the vents. Using the more probable assumption that water is entrained continuously throughout the plume's rise requires a higher percentage of entrained water and less ambient water. In Table 3, I use these mixture percentages and the assumption that the entrained water has a manganese concentration of 50 nmoles Mn/kg (Figure 11) to predict the manganese concentration in the neutrally buoyant plume over the vent field. It can be seen that diffuse, low-temperature venting (the entrained water) may be responsible for approximately 50% or more of the fluxes of manganese and heat from the vent field. It should be noted that the predicted manganese concentration in the neutrally buoyant plume is very sensitive to the assumed percentage of vent water, a small number that is not known with great precision. However, the maximum (plume core) and average manganese concentrations of the four vent field stations, listed in Table 4, show excellent agreement with the calculated manganese concentration in Table 3.

IV. Manganese Oxidation and Removal Rates

Although I have shown that relatively little manganese is lost during the buoyant phase of the plume, both sediment trap studies (Dymond and Roth, 1988) and sediment analyses (Dymond, 1981; Massoth, et al., 1984) clearly show removal of manganese from the neutrally buoyant plume. These observations are consistent as it can be

Table 3

Calculation of Neutrally Buoyant Plume [Mn]

Source	% Contribution		Concentration		Contribution to Final Mn Conc.
Vents	0.01%	x	300 mM	=	30.0 nM
Ambient	30%	x	1 nM	=	0.3 nM
Entrained	70%	x	50 nM	=	35.0 nM
			Total [Mn]	=	65.3 nM

Table 4

Endeavour Ridge Vent Field Stations [Mn]

Hydrocast	Average [Mn], nmole/kg	Plume core [Mn], nmole/kg
P2CTD1	59.1	77
P2CTD3	42.8	52
P2CTD12	47.7	65
P2CTD15	52.5	75
Average	50.5	67

shown that the amount of manganese removal required to make up the measured fluxes can be accounted for by an undetectable loss from the plume. This calculation is shown for both manganese and iron in Appendix C.

Manganese does not oxidize in the absence of oxide or bacterial surfaces (Diem and Stumm, 1984). However, in the presence of such surfaces, Mn(II) is adsorbed to a surface and is then slowly oxidized over approximately 48 hours (Hastings and Emerson, 1986). With my methods, I cannot make a distinction between adsorbed manganese that is reduced and that which is oxidized. Therefore, I will calculate an adsorption/oxidation rate, but I will refer to it as an oxidation rate. Once manganese is associated with particles, it can be removed from the plume by incorporation into fecal material and/or gravitational settling. The oxidation and removal rates of manganese can be estimated by comparing the dissolved and total Mn/ΔT ratios, respectively, at increasing distances "downplume." If manganese is being oxidized, the dissolved Mn/ΔT ratio should decrease downplume. Removal of manganese is demonstrated by decreasing total Mn/ΔT ratios. If the particle removal rate is fast relative to the oxidation rate, the dissolved manganese concentration should remain equal to the total manganese concentration. However, if the particle removal rate is slow relative to the oxidation rate, particulate manganese should be present in downplume samples.

In Table 2, it can be seen that both total and dissolved Mn/ΔT ratios decrease downplume. Dissolved Mn/ΔT decreases ~700 nmoles Mn/kg/°C and total Mn/ΔT decreases ~400 nmoles Mn/kg/°C from the vent field to the 17-km stations. This data can be presented as losses from the plume (Figure 12) by subtracting each station's Mn/ΔT ratio from an initial 1500 nmoles/kg/°C. As pointed out previously, current flow regimes are complex in and around the ridge crest. Current velocities of 2 to 5 cm/second have been measured at the Endeavour Ridge vent field (Dymond and Roth, 1988). If I assume a current velocity of 1 cm/second, approximately 500 hours would be required for the plume to advect 17 km. Directional deviations and tidal oscillations can reduce this velocity and therefore increase the advection time, but

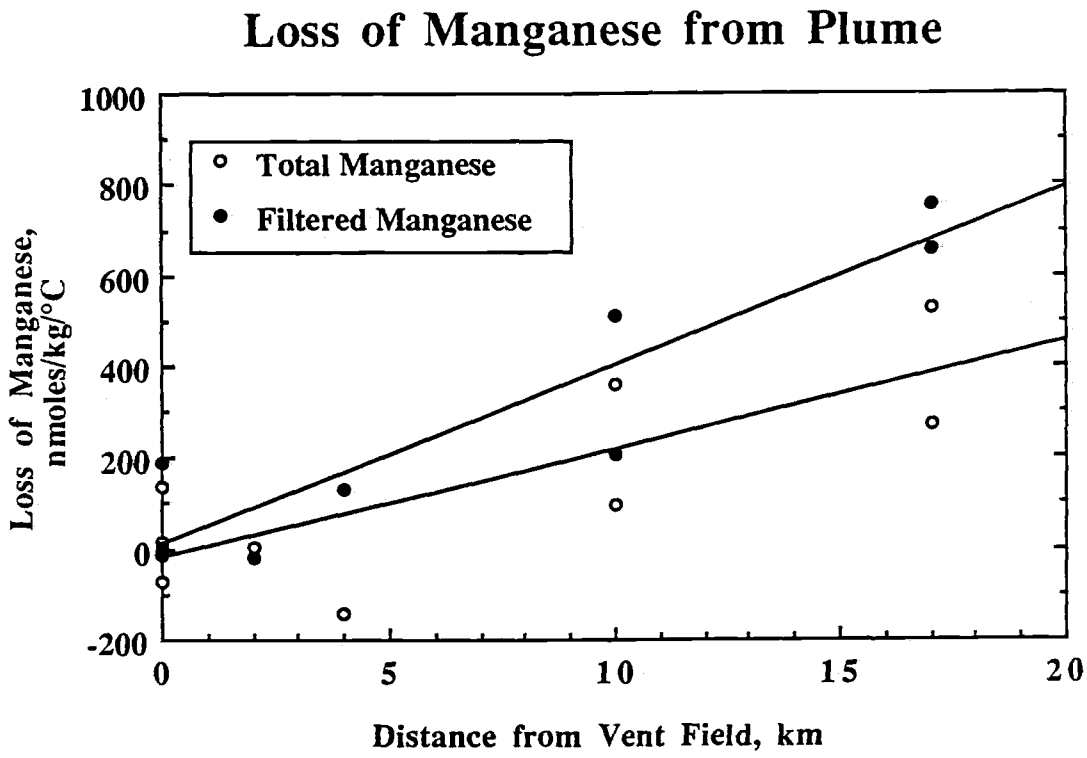

Figure 12. The loss of manganese from the advecting plume. The Mn/ΔT ratio of each station is subtracted from the average vent field Mn/ΔT ratio of 1500 nmoles/kg/°C. The lines shown are linear regressions for the loss of total (open circles) and filtered (solid circles) manganese.

this calculation is strictly an "order of magnitude" calculation. The decrease in dissolved Mn/ΔT of ~ 700 nmoles Mn/kg/°C over 500 hours represents an oxidation rate of ~1.3 x 10^{-11} moles Mn/kg/hr. The decrease in total Mn/ΔT of ~400 nmoles Mn/kg/°C represents a removal rate of ~0.8 x 10^{-11} moles Mn/kg/hr.

The oxidation rate catalyzed by oxide surfaces can be estimated by using the rate law suggested for the oxidation of manganese on γ-FeOOH (lepidocrocite) (Sung and Morgan, 1981):

$$\frac{-\,d[Mn(II)]}{dt} = k^* [OH^-]^2 [Fe(III)_T] [Mn(II)] [O_2] \qquad (3)$$

where k* is the rate constant, equal to 2.0 ($\pm$0.8) x 10^{18} $\underline{M}^{-4}$·day^{-1}, $[OH^-]$ is the hydroxide concentration, $[O_2]$ is the dissolved oxygen concentration [Mn(II)] is the dissolved manganese concentration, and $[Fe(III)_T]$ is the total concentration of iron. A similar rate law has been used to describe the autocatalytic oxidation of manganese on MnO_2 (Brewer, 1975). Using equation (3) and representative parameters for our area, the abiotic oxidation rate of manganese is estimated to range from 10^{-16} to 10^{-14} moles Mn/kg/hr. In laboratory experiments, manganese oxidation rates catalyzed by bacterial surfaces have been estimated to be four orders of magnitude greater than those on manganese and iron oxide surfaces (Hastings and Emerson, 1986). Therefore, initial bacterial oxidation rates of 10^{-12} to 10^{-10} moles Mn/kg/hr could be expected. The calculated adsorption/oxidation rates of 10^{-11} moles Mn/kg/hr, are in the middle of this range, suggesting that bacteria may be mediating the oxidation of manganese in the Endeavour Ridge plume.

I can also compare this observed loss to measured bacterially-mediated oxidation rates in hydrothermal plumes. Scavenging rate constants (k_1) ranging from approximately 1 to 3 yr^{-1} were measured 16 to 20 km from the ridge crest in the neutrally buoyant plume at the Cleft Segment of the southern Juan de Fuca Ridge (Cowen, et al., 1990). By running parallel poisoned and non-poisoned experiments, the scavenging rate was determined to be primarily due to active bacteria. The

scavenging rate constants at Endeavour Ridge can be estimated by assuming (a) the oxidation reaction is described as:

$$\text{Dissolved Mn (DMn)} \xrightarrow{k_1} \text{Particulate Mn (PMn)} \qquad (4)$$

and (b) the reverse desorption/dissolution reaction is negligible. Therefore:

$$k_1 = \frac{[PMn]_t}{[DMn]_0 \cdot t} \qquad (5)$$

where k_1 is the scavenging rate constant, t is time, $[DMn]_0$ is the initial manganese concentration, and $[PMn]_t$ is the particulate manganese concentration at time "t." Using equation (5), the scavenging rate constant for Endeavour Ridge is calculated to be ~2 yr^{-1} at the 17-km stations. The agreement between these rates and those at the southern Juan de Fuca Ridge supports the view that the manganese oxidation mechanism at Endeavour Ridge is bacterially mediated. The rate constant will vary with temperature and bacterial cell concentration. However, deep-sea temperature is very constant at ~2° C, and both sets of data are from similar distances from the ridge crests, and hopefully, have similar bacterial morphologies and cell counts.

Bacterial oxidation has been invoked previously to explain the removal or scavenging of manganese from hydrothermal plumes (Campbell, et al., 1988; Cowen, et al., 1986; Cowen, et al., 1990; Cowen and Silver, 1984). According to Cowen and Li, 1990, the bacterial community at the southern Juan de Fuca Ridge changes from the vent field to far-field stations. At Endeavour Ridge, there is a changing bacterial community also. Figure 13 shows the changes both in cell counts and morphology. The samples taken near the vent field are characterized by cocci, ~ 1μm in diameter, and lower cell counts. The 17-km stations have higher cell counts, with sheathed, rod-shaped bacteria (10 -15 μm in diameter) similar to those typically identified as "metal-oxidizing." The rods coagulate in masses hundreds of microns in

Figure 13. Bacterial morphology of samples and bacterial cell counts from plume. Note absence of cocci and coagulation of rod-shaped bacteria in samples from 17-km stations. Bar is 10 μm in length. This figure and the bacterial analysis was made by J. Baross and M. D. Lilley at the University of Washington.

Figure 13 - Bacterial Morphology And Cell Counts

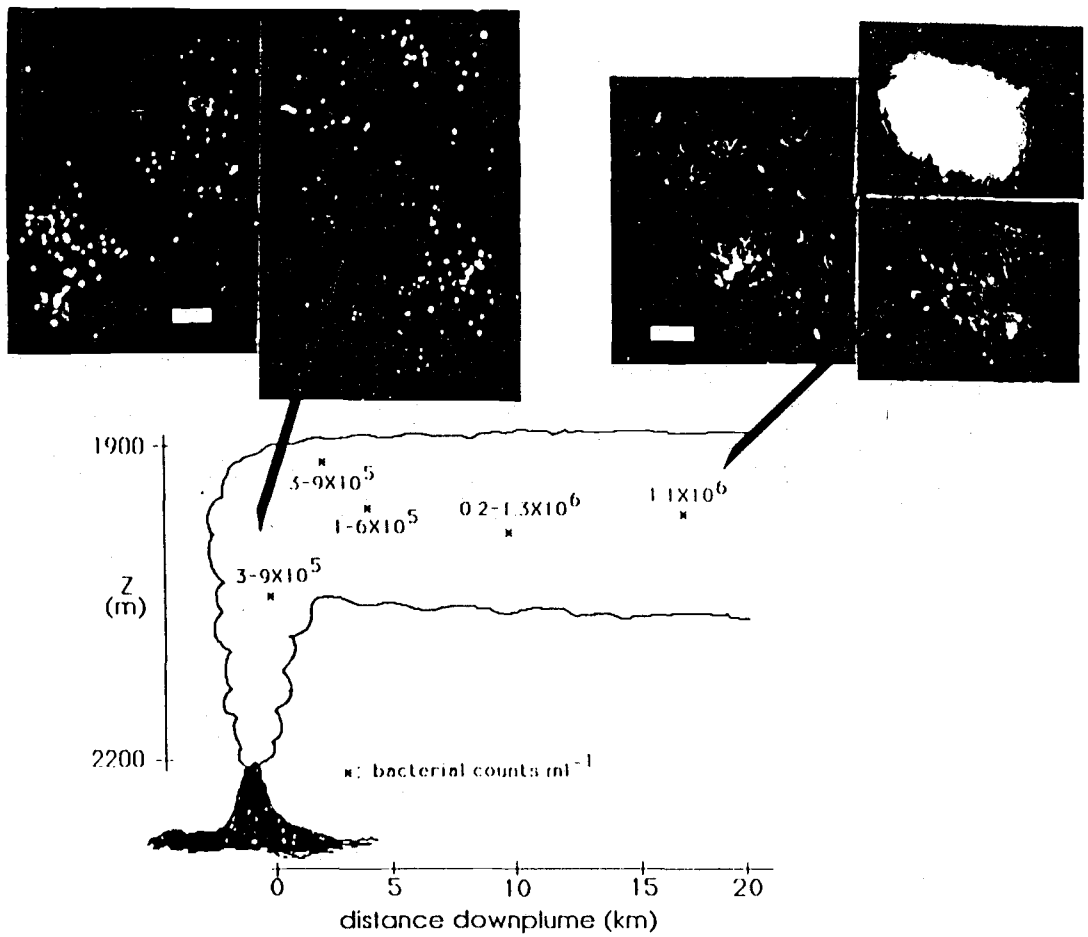

diameter, which might further enhance their removal from the water column. These masses of bacteria are coated with manganese (J. Baross and M. D. Lilley, pers. comm.). It is possible that it either takes some time for the rods to "grow in" or there is something inhibiting their growth near the vent fields. However, if the "grow in" theory is correct, it seems that eventually these bacteria would "grow in" at the vent field. It makes more sense if there is an inhibitory agent. If this is true, it would be interesting to compare neutrally buoyant plume waters from Guaymas Basin with that from other vent fields and see if there is an inhibitory agent. By the same reasoning, whatever the cocci are feeding on must be consumed near the vent field, or there is an inhibitory agent in the far-field waters. Here, it makes more sense if their food supply is consumed. It is doubtful that an inhibitory agent would "grow in" during the plume's advection.

In summary, I find a manganese adsorption/oxidation rate similar to rates that are bacterially-mediated. The bacterial morphology changes from the cocci at the vent field to rod-shaped bacteria that are similar to "metal-oxidizing" bacteria and are coated with manganese.

V. Light Anomaly and Iron Removal

I've shown that manganese behaves nearly conservatively near the vent field. In order to examine processes closer to the vent field, tracers such as iron concentration and particle concentration must be considered. Light absorbance, or light anomaly, is an indicator of the particle concentration. Figure 14 is a plot of light anomaly (in m^{-1}) vs. ΔT for a tow-yo cast, whose track is shown in Figure 1. The data for this tow-yo is used as it illustrates the behavior of all of the other hydrocasts. Two regions can clearly be seen: (a) a region exhibiting a nearly linear relationship, found in the distal plume and ending in background water, and (b) a region exhibiting a non-linear relationship,which was found only directly over the vent field. Light absorbance is affected by particle concentration and particle size distribution. This allows two possible explanations to explain the difference in vent field and far-field

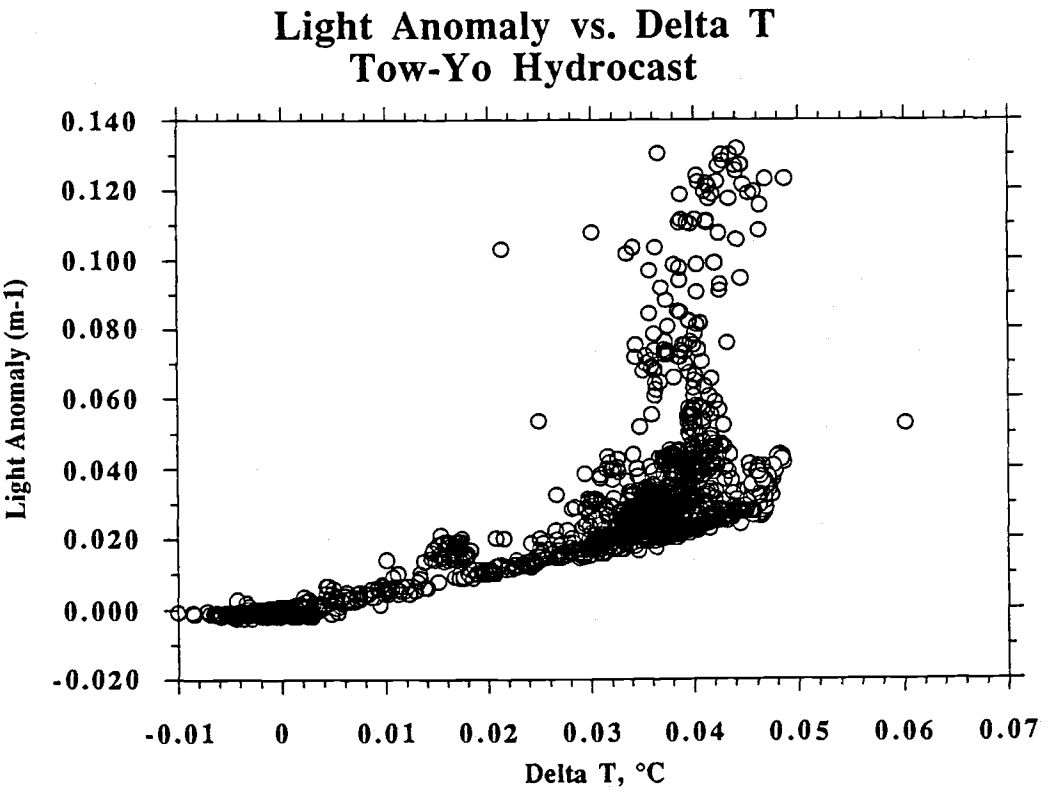

Figure 14. Light Anomaly (m^{-1}) vs. ΔT for Tow-Yo hydrocast. Note almost linear relationship at lower ΔTs and light anomalies. The track of the tow-yo is shown in Figure 1.

observations. The explanations are not mutually exclusive, and both are probably occurring.

The first is that there is something causing the light absorbance at the vent field that is not present in the far-field plume. de Angelis, 1989 measured methane oxidation at the Endeavour Ridge vent field and in the neutrally buoyant plume. The methanotrophs may be responsible for the increased light absorbance at the vent field. They would be absent from the far-field plume due to the lack of dissolved methane. This explanation would also support the change in bacterial morphology found between the vent field and the 17-km stations. The metal sulfides emitted by the hydrothermal vents that settle rapidly could also cause the increased light absorbance at the vent field. However, their large size, indicated by their rapid settling times, would suggest that their light absorbance (Baker and Lavelle, 1984.) It is possible that their irregular and angular shapes may cause increased light refraction, though.

The second is that particles are smaller at the vent field and are aggregated as they are advected away. Campbell, et al., 1990 suggests that iron phases are the major light-attenuating particles at the vent field. If this is true, examination of the relationships between iron and light attenuation should help explain the observations. Figure 15 is a plot of light anomaly vs. total iron concentration of vent field samples and far-field samples, with a linear regression for far-field samples. Samples from the vent field have a higher light absorbance than expected from their iron concentration. In Figure 16 it can be seen that for light anomalies greater than 0.03 m^{-1} (vent field samples), there is an inverse relationship between light anomaly and the % Particulate Fe. The scattering of points with light anomaly ~0 are far-field samples whose low iron concentrations cause reduced accuracy in calculating % Particulate Fe. Samples with a greater concentration of dissolved iron (non-filterable) have larger light anomalies. This suggests a simple case of smaller particles scattering light more effectively than larger particles (Baker and Lavelle, 1984). Particle size distributions have been determined using a Coulter counter at Endeavour Ridge and at the southern Juan de Fuca Ridge (Walker and Baker, 1988). These investigators noted that samples taken from water with higher light

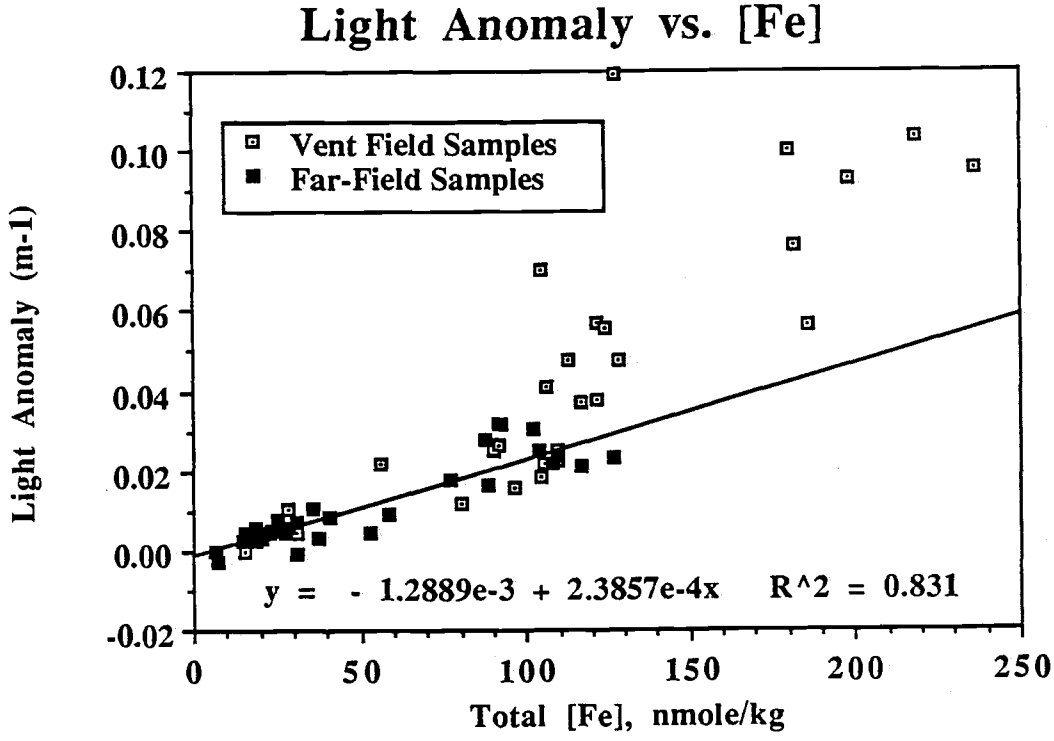

Figure 15. Light Anomaly (m^{-1}) vs. total [Fe] for all samples. The linear correlation shown is only for far-field samples (solid squares). The vent field samples clearly have greater light anomaly relative to their iron concentration.

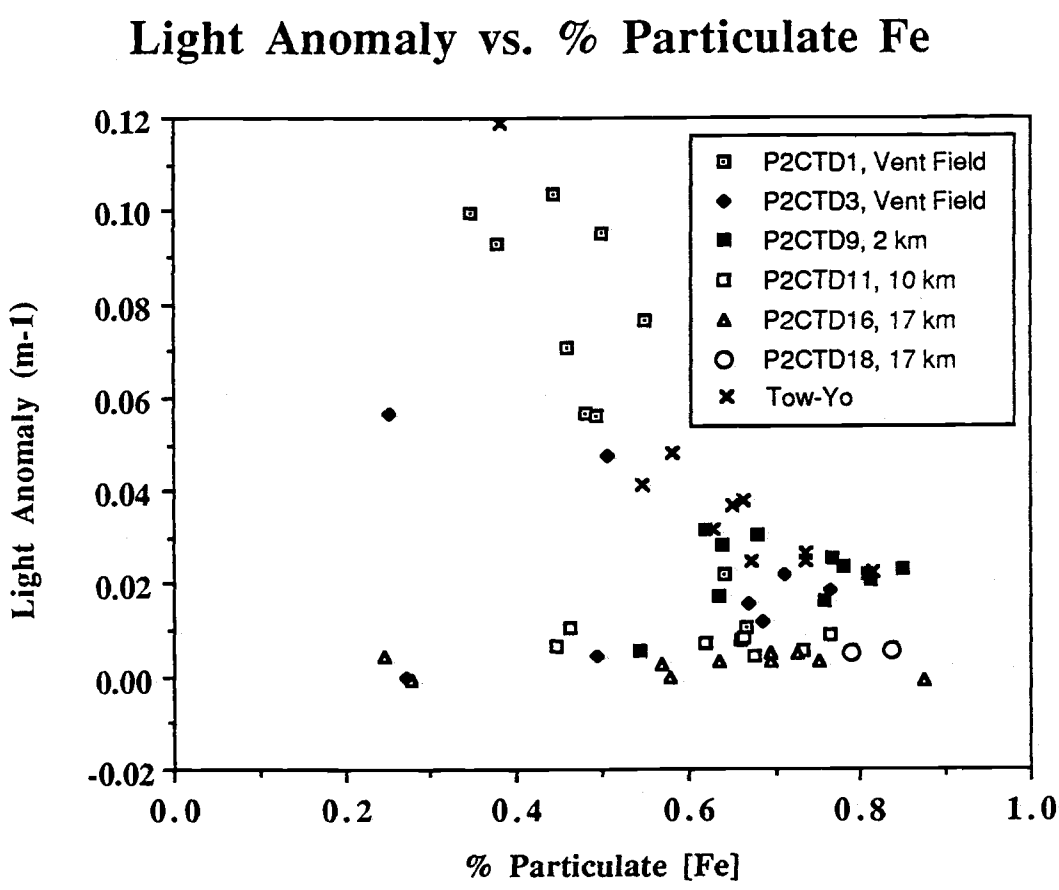

Figure 16. Light Anomaly (m^{-1}) vs. % particulate [Fe]. The vent field samples show a negative correlation between these two parameters.

anomalies (greater than 0.06 m^{-1}) had particle distributions with smaller median diameters. As distance from the vent field increased, the median diameter increased.

This implies some aggregation mechanism. My study was not designed to discern such a mechanism, but I can hypothesize about it. Dymond and Roth, 1988 suggested that zooplankton filtration may be responsible for the aggregation of ~2 μm diameter particles. Honeyman and Santschi, 1989 suggest that while biotic filtering may be responsible for the aggregation of micron-sized particles, "Brownian pumping" may cause aggregation of submicron-sized particles. Brownian pumping is the transfer of dissolved metal species to filterable particles through a colloidal intermediate. The reduced iron emerging from hydrothermal vents is generally thought to rapidly oxidize. Campbell, et al., 1990 has observed iron oxyhydroxide particles ~1 to 20 nm in diameter. So, it is possible that the large shear velocities and colloidal population in the vent field region contributes to a rapid aggregation of the submicron-diameter particles. As they are transfered into the filterable particle sizes, zooplankton filtration may remove them from the water column. As the plume advects away from the vent field, the shear velocities are reduced and therefore particle aggregation of the submicron-diameter particles should be reduced. Support for this suggestion can be seen in Table 2 and in Figure 17. The dissolved Fe/ΔT ratio decreases rapidly between the vent field and the 2-km station. The total Fe/ΔT ratio decreases rapidly during this interval, also. This implies both a rapid aggregation method and a rapid removal method once the particles are aggregated. However, downplume of the 2-km station, the dissolved Fe/ΔT ratio remains fairly constant. If Brownian pumping is responsible for the aggregation of the submicron-diameter particles, its driving force is reduced or even absent in the far-field plume. Since there is no mechanism to move the particles into the zooplankton-filtering size, zooplankton populations may be reduced.

This has implications for the bacterial masses that J. Baross and M. D. Lilley have found that are coated with manganese. Why are they there? These should be great food sources for zooplankton. But if the zooplankton are confined to the vent field area, due to the requisite shear

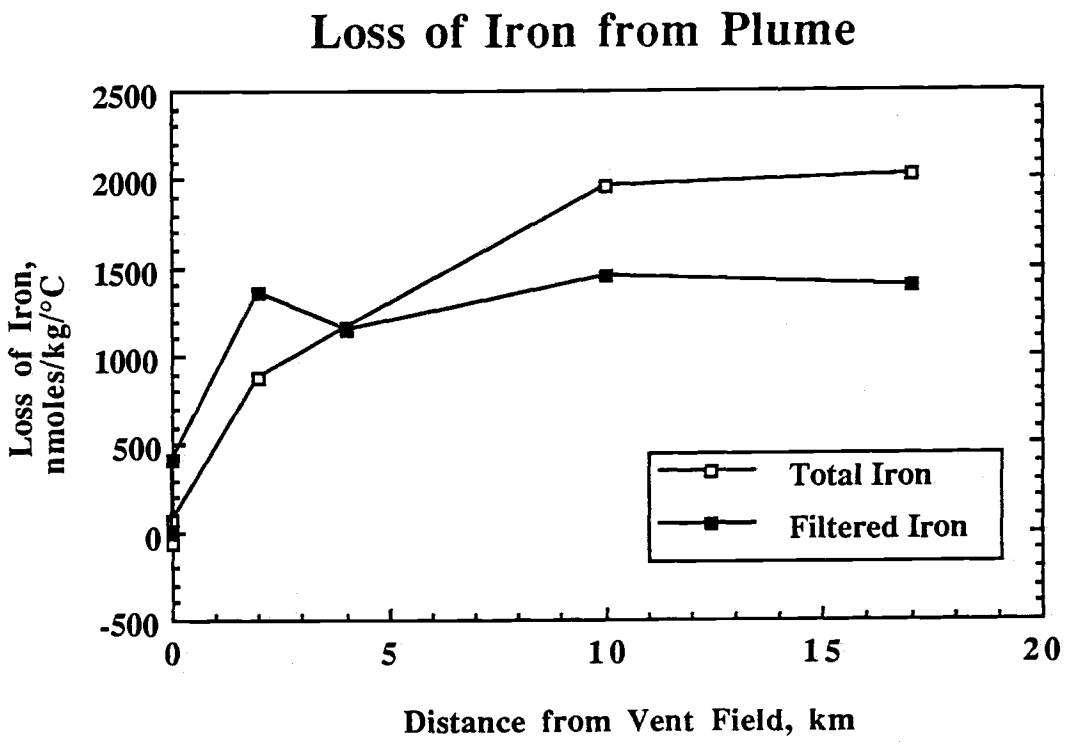

Figure 17. Loss of iron from plume (similar to Figure 12 for manganese). The iron loss was calculated by subtracting each station's Fe/ΔT ratio from the average vent field ratio of 3672 nmoles/kg/°C.

forces for aggregating the submicron-diameter particles, farther away from the vent field, the bacterial masses are allowed to grow and aggregate. It is possible that the zooplankton are the inhibitory agent preventing the growth of a metal-oxidizing bacterial population at the vent field.

From the previous discussion, it can be seen that the process of filtering produces a size fractionation rather than a distinction between "reduced" and "oxidized." Since an oxidation rate cannot be calculated for iron with my data, only an iron removal rate has been estimated. The total Fe/ΔT ratio decreases from ~3700 nmoles Fe/kg/°C at the vent field to 1650 nmoles Fe/kg/°C at the 17-km station, a loss of ~2050 nmoles Fe/kg/°C (Table 2). This translates to an average removal rate over the 17 km distance of ~4 x 10^{-11} moles Fe/kg/hr. However, the removal rate is not constant, being much higher near the vent field (Figure 17). More than 40% of the total iron removal occurs within 2 km of the vent field and over 95% occurs within 10 km. Although the removal of iron seems to cease after 10 km, this could be due to under-estimation of ΔT at the 17-km stations and/or inability to detect small losses of iron at the 17-km stations. I can calculate a first-order rate constant for the removal of iron in the same manner that the rate constant for manganese oxidation was calculated (equation 5) by:

$$k_1 = \frac{[Fe]_{T-0} - [Fe]_{T-t}}{[Fe]_{T-0} \times t} \qquad (6)$$

where $[Fe]_{T-0}$ is the total average iron concentration at the vent field stations, $[Fe]_{T-t}$ is the total average iron concentration at time t, and t is time. Using the values from Tabel 2, $[Fe]_{T-0}$ = 156 nmoles/kg (from P2CTD1), $[Fe]_{T-t}$ = 15 nmoles/kg (from P2CTD16), and t = 500 hours, k_1 = .002 hr^{-1} or ~18 yr^{-1}.

VI. Fe/Mn Ratios

The different removal rates of iron and manganese result in a fractionation of the two metals on particulate matter, which affects the Fe/Mn ratio of the sediments underlying the advecting plume. Hydrothermally-influenced sediments located near the ridge crests and suspended particles have Fe/Mn ratios ranging from 2 to 9, with an average of ~3.5 (Dymond, 1981; Hudson, 1984; Hudson, et al., 1986; Massoth, et al., 1984). Axial valley sediments and settling particles are generally much higher (Dymond and Roth, 1988; Massoth, et al., 1984).

Vent fluids at Endeavour Ridge have an Fe:Mn ratio of approximately 3:1 [D. Butterfield, pers. comm.] Total iron concentration is plotted against total manganese concentration for all samples taken in the neutrally buoyant plume in Figure 18. It can be seen that iron is non-conservative relative to manganese. The Fe/Mn ratios of the particles lost from the advecting plume have been calculated by using the linear relationships for manganese in Figure 12 and the actual data for iron from Table 2. The actual data for manganese was not used since the apparent "gain" in total manganese at the 4-km station (Figure 12) would give a negative Fe/Mn ratio. The reason for the "gain" is unknown. It is possible that there is a vent field located to the south of the Endeavour Ridge vent field with a different Mn/ΔT ratio that was contributing to the plume at this station. This station is located very close to the ridge crest. These average ratios of the particles lost between stations are shown in Figure 19 as stipled areas, and they are similar to the Fe/Mn ratios of surface sediments (points) from a transect across the southern Juan de Fuca Ridge (Massoth, et al., 1984). The Fe/Mn ratio for the overall loss of iron and manganese by the time the plume has advected 17 km is 5:1.

In summary, there is a fractionation of iron and manganese during the advection of the neutrally buoyant plume. Within my region of study, iron is removed faster initially, which should result in a constantly decreasing Fe/Mn ratio in the sediments underlying the advecting plume. The Fe/Mn ratio of the particles lost from the plume is within the characteristic range of hydrothermally-influenced sediments.

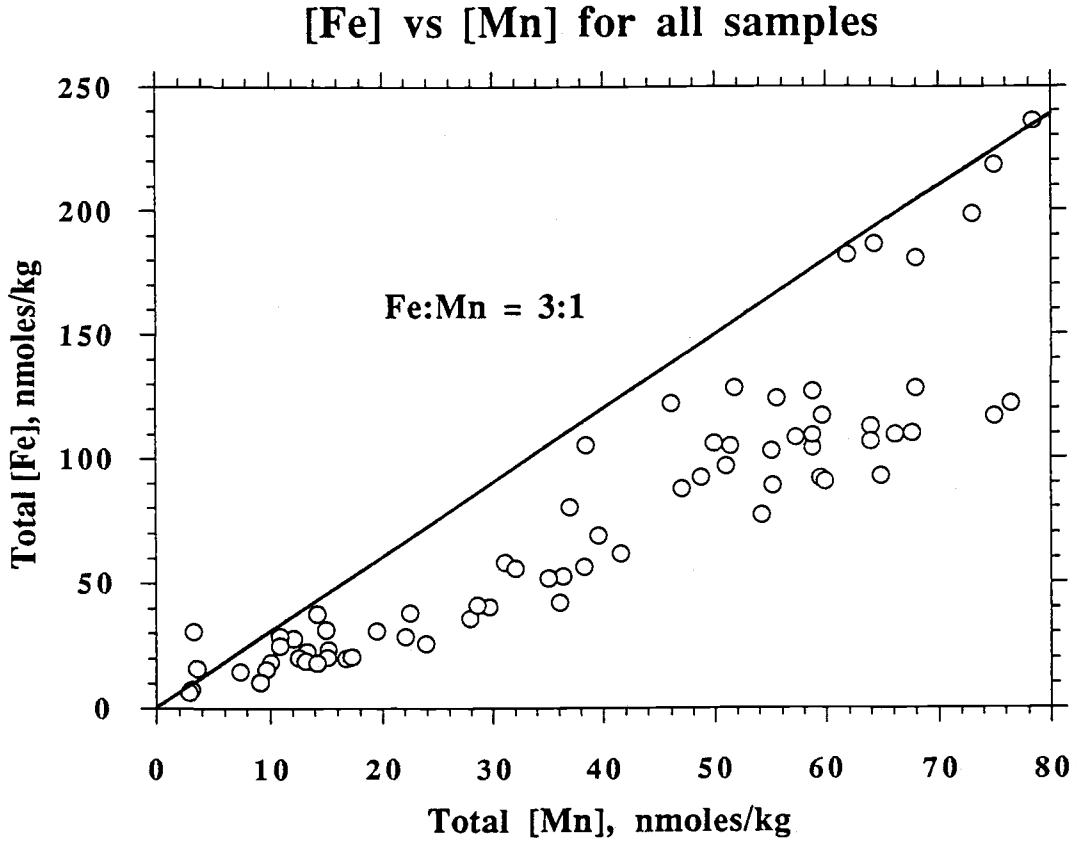

Figure 18. Total [Fe] vs. total [Mn] for all samples. A line is drawn illustrating the average high-temperature vent ratio of 3:1 Fe:Mn.

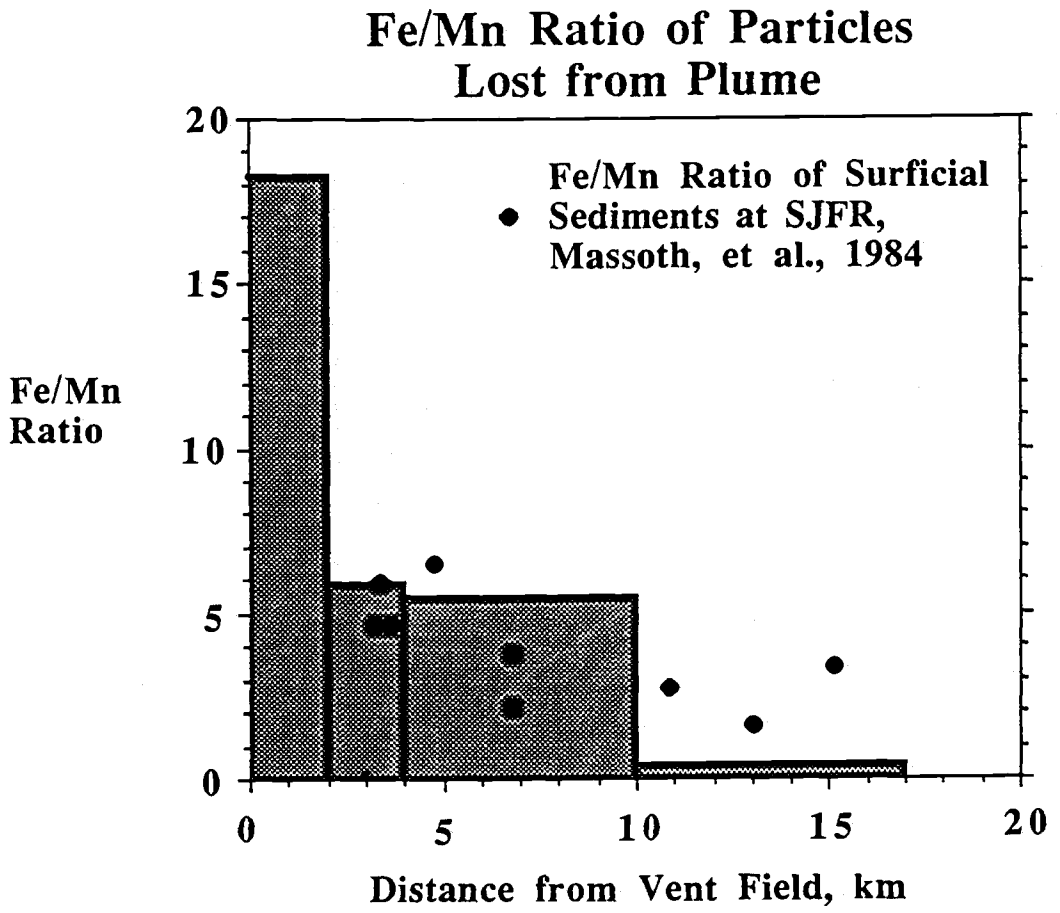

Figure 19. Fe/Mn ratios of the particles lost from the plume vs. distance from the vent field. Hatched areas shown are averages between stations. Points indicate Fe/Mn ratios from a transect across the southern Juan de Fuca Ridge. The graph does not include a Fe/Mn ratio of 267 found on the ridge crest (Massoth, et al., 1984).

CONCLUSIONS

Many variables affect the estimation of the heat content of a neutrally buoyant plume. Entrainment, extreme dilution, varying source fluids and source strengths, and non-linear background fields of temperature and salinity all add to the uncertainty. However, I estimate that the Mn/ΔT ratio in the neutrally buoyant plume at Endeavour Ridge is indistinguishable from that found in the source vents. This suggests that little manganese is lost during the buoyant rise of the plume. However, the high-temperature vents are not the sole source of either manganese or heat to the neutrally buoyant plume.

Manganese is transferred to filterable particle size ranges at a rate of ~1.3 x 10^{-11} moles Mn/kg/hr, which is consistent with bacterial oxidation rates. The bacterial morphology of plume samples changes from ~1 μm cocci over the vent field to 10 -15 μm filamentous, sheathed bacteria in large aggregates at the 17-km stations. Further experiments are planned to determine whether these filamentous bacteria are manganese-coated. Manganese is removed from the neutrally buoyant plume at a rate of ~0.8 x 10^{-11} moles Mn/kg/hr.

Increased light anomalies over the vent field appear to be due to greater number of smaller particles. A large percentage of these submicron diameter particles are rapidly aggregated and removed within a few kilometers. The removal rate of iron varies, with the highest rates near the vent field. At distances greater than 10 km, the removal rate of iron was below our detection limit. The average removal rate for iron is ~4 x 10^{-11} moles Fe/kg/hr.

The different removal rates of iron and manganese fractionate the two metals and result in a continuously decreasing Fe/Mn ratio of the particles removed from the neutrally buoyant plume. The overall Fe/Mn ratio of the particles that are lost from the neutrally buoyant plume during its advection from the vent field to the 17-km stations is 5:1, within the characteristic range of hydrothermal sediments

BIBLIOGRAPHY

de Angelis, M., 1989, "Studies of Microbial Methane Oxidation in Deep-Sea Hydrothermal Vent Environments", Ph.D. Thesis, University of Washington, Seattle, Washington.

Baker, E. T. and J. W. Lavelle, 1984, "The Effect of Particle Size on the Light Attenuation Coefficient of Natural Suspensions", Journal of Geophysical Research, **89**: 8197-8203.

Baker, E. T., J. W. Lavelle, R. A. Feely, G. J. Massoth and S. L. Walker, 1989, "Episodic Venting of Hydrothermal Fluids From the Juan de Fuca Ridge", Journal of Geophysical Research, **94**: 9237-9250.

Baker, E. T. and G. J. Massoth, 1986, "Hydrothermal Plume Measurements: A Regional Perspective", Science, **234**: 980-982.

Baker, E. T. and G. J. Massoth, 1987, "Characteristics of hydrothermal plumes from two vent fields on the Juan de Fuca Ridge, northeast Pacific Ocean", Earth and Planetary Science Letters, **85**: 59-73.

Baker, E. T., R. E. McDuff and G. J. Massoth, 1990, "Hydrothermal Venting from the Summit of a Ridge Axis Seamount: Axial Volcano, Juan de Fuca Ridge", Journal of Geophysical Research, **95**: 12843-12854.

Brewer, P. G., 1975, "Minor Elements in Seawater", in Chemical Oceanography, **1**: 445-496.

Campbell, A. C., R. G. Burns, J. M. Edmond, H. Elderfield and M. Greaves, 1990, "Chemistry and Mineralogy of Buoyant Hydrothermal Plume Particles: TAG and MARK Vents Mid-Atlantic Ridge", EOS, **71**: 1651.

Campbell, A. C., J. M. Gieskes, J. E. Lupton and P. F. Lonsdale, 1988, "Manganese geochemistry in the Guaymas Basin, Gulf of California", Geochimica et Cosmochimica Acta, **52**: 345-357.

Campbell, I. H., T. J. McDougall and J. S. Turner, 1984, "A note on fluid dynamic processes which can influence the deposition of massive sulfides", Economic Geology, **79**: 1905-1913.

Cann, J. R. and M. R. Strens, 1989, "Modeling Periodic Megaplume Emission by Black Smoker Systems", Journal of Geophysical Research, **94**: 12227-12237.

Cannon, G. A., E. T. Baker, D. J. Pashinski and M. Lemon, 1990, "Variations in Off-axis Currents and Water Properties Related to the Fate of Hydrothermal Effluents", EOS, **71**: 1619.

Cannon, G. A. and D. J. Pahinski, 1990, "Circulation Near Axial Seamount", Journal of Geophysical Research, **95**: 12823-12828.

Cowen, J. P. and Y. H. Li, 1990, "The Influence of a Changing Bacterial Community on Trace Metal Scavenging in a Deep-Sea Particle Plume", Submitted to Journal of Marine Research,

Cowen, J. P., G. J. Massoth and E. T. Baker, 1986, "Bacterial Scavenging of Mn and Fe in a mid-to far-field hydrothermal Particulate Plume", Nature, **322**: 169-171.

Cowen, J. P., G. J. Massoth and R. A. Feely, 1990, "Scavenging Rates of Dissolved Manganese in a Hydrothermal Vent Plume", submitted to Deep-Sea Research.

Cowen, J. P. and M. W. Silver, 1984, "The Association of Fe and Mn with Bacteria on Marine Macroparticulate Material", Science, **224**: 1340-1342.

Diem, D. and W. Stumm, 1984, "Is dissolved Mn2+ being oxidized by O2 in absence of Mn-bacteria or surface catalysts?", Geochimica et Cosmochimica Acta, **48**: 1571-1573.

Dymond, J., 1981, "Geochemistry of Nazca plate surface sediments: An evaluation of hydrothermal, biogenic, detrital, and hydrogeneous sources", in Nazca Plate: Crustal Formation and Andean Convergence, **154**: 133-174.

Dymond, J. and S. E. Roth, 1988, "Plume dispersed hydrothermal particles: A time-series record of settling flux from the Endeavour Ridge using moored sensors", Geochimica et Cosmochimica Acta, **52**: 2525-2536.

Elderfield, H., M. Godfrey, A. Mitra and M. Rudnicki, 1990, "Chemical Dynamics of the TAG Hydrothermal Plume, 26° N, Mid-Atlantic Ridge", EOS, **71**: 1651.

Hammond, S. R., J. S. Lee, A. Malahoff, R. Feely and R. W. Embley, 1984, "Discovery of High-Temperature Hydrothermal Venting On The Endeavour Segment of the Juan De Fuca Ridge", EOS, **65**: 1111.

Hastings, D. and S. Emerson, 1986, "Oxidation of manganese by spores of a marine bacillus: Kinetic and thermodynamic considerations", Geochimica et Cosmochimica Acta, **50**: 1819-1824.

Honeyman, B. D., and P. H. Santschi, 1989, "A Brownian-pumping model for oceanic trace metal scavenging: Evidence from Th isotopes," Journal of Marine Research, **47**:951-992.

Hudson, A., 1984, "Hydrothermal Iron in Seawater Around the East Pacific Rise", EOS, **65**: 974.

Hudson, A., M. L. Bender and D. W. Graham, 1986, "Iron enrichments in hydrothermal plumes over the East Pacific Rise", Earth and Planetary Science Letters, **79**: 250-254.

Kadko, D., N. D. Rosenberg, J. E. Lupton, R. W. Collier and M. D. Lilley, 1990, "Chemical Reaction Rates and Entrainment within the Endeavour Ridge Hydrothermal Plume", Earth and Planetary Science Letters, **99**: 315-335.

Klinkhammer, G., H. Elderfield, M. Greaves, P. Rona and T. Nelsen, 1986, "Manganese geochemistry near high-temperature vents in

the Mid-Atlantic Ridge rift valley", Earth and Planetary Science Letters, **80**: 230-240.

Klinkhammer, G. P., 1980, "Determination of Manganese in Seawater by Flameless Atomic Absorption Spectrometry after Pre-concentration with 8-Hydroxyquinoline in Chloroform", Analytical Chemistry, **52**: 117-120.

Landing, W. M. and K. W. Bruland, 1987, "The contrasting biogeochemistry of iron and manganese in the Pacific Ocean", Geochimica et Cosmochimica Acta, **51**: 29-43.

Lilley, M. D., J. A. Baross and L. I. Gordon, 1983, "Reduced gases and bacteria in hydrothermal fluids: The Galapagos Spreading Center and 21° N East Pacific Rise", in Hydrothermal processes at seafloor spreading centers, 411-450.

List, E. J., 1982, "Turbulent Jets and Plumes", Annual Review of Fluid Mechanics, **14**: 189-212.

Little, S. A., K. D. Stolzenbach and R. P. Von Herzen, 1987, "Measurements of Plume Flow From a Hydrothermal Vent Field", Journal of Geophysical Research, **92**: 2587-2596.

Lupton, J. E., 1990, "Water Column Hydrothermal Plumes on the Juan de Fuca Ridge", Journal of Geophysical Research, **95**: 12829-12842.

Lupton, J. E., E. T. Baker and G. J. Massoth, 1989, "Variable 3He/heat ratios in submarine hydrothermal systems: evidence from two plumes over the Juan de Fuca ridge", Nature, **337**: 161-164.

Lupton, J. E., J. R. Delaney, H. P. Johnson and M. K. Tivey, 1985, "Entrainment and vertical transport of deep-ocean water by buoyant hydrothermal plumes", Nature, **316**: 621-623.

Lupton, J. E., G. P. Klinkhammer, W. R. Normark, R. Haymon, K. C. MacDonald, R. F. Weiss and H. Craig, 1980, "Helium-3 and manganese at the 21 °N East Pacific Rise hydrothermal site", Earth and Planetary Science Letters, **50**: 115-127.

Massoth, G. J., E. T. Baker, R. A. Feely and H. C. Curl Jr., 1984, "Hydrothermal Signals Away from the SJFR", EOS, **65**: 1112.

McDougall, T. J., 1990, "Bulk properties of "hot smoker" plumes", Earth and Planetary Science Letters, **99**: 185-194.

McDuff, R. E., 1988, "Effects of Vent Fluid Properties on the Hydrography of Hydrothermal Plumes", EOS, **69**: 1497.

Middleton, J. H., 1979, "Times of rise for turbulent forced plumes", Tellus, **31**: 82-88.

Middleton, J. H., 1986, "The rise of forced plumes in a stably stratified crossflow", Boundary-Layer Meteorology, **36**: 187-199.

Morton, B. R., 1959, "Forced plumes", Journal of Fluid Mechanics, **5**: 151-163.

Morton, B. R. and J. Middleton, 1973, "Scale diagrams for forced plumes", Journal of Fluid Mechanics, **58**: 165-176.

Morton, B. R., S. G. Taylor F. R. S. and J. S. Turner, 1956, "Turbulent gravitational convection from maintained and instantaneous sources", Proceedings of the Royal Society, **234A**: 1-23.

Mottl, M. J. and T. F. McConachy, 1990, "Chemical processes in buoyant hydrothermal plumes on the East Pacific Rise near 21 °N", Geochimica et Cosmochimica Acta, **54**: 1911-1927.

Norton, D. L., 1984, "Theory of hydrothermal systems", in Annual Review of Earth and Planetary Science, **12**: 155-177.

Rona, P. A. and D. A. Trivett, 1990, "Discrete and Diffuse Heat Transfer at ASHES Vent Field, Axial Volcano, Juan de Fuca Ridge", EOS, **71**: 1570.

Rosenberg, N. D., J. E. Lupton, D. Kadko, R. Collier, M. D. Lilley and H. Pak, 1988, "Estimation of heat and chemical fluxes from a seafloor hydrothermal vent field using radon measurements", Nature, **334**: 604-607.

Roth, S. E. and J. Dymond, 1989, "Transport and settling of organic material in a deep-sea hydrothermal plume: evidence from particle flux measurements", Deep-Sea Research, **36**: 1237-1254.

Rouse, H., C. S. Yih and H. W. Humphreys, 1952, "Gravitational Convection from a Boundary Source", Tellus, **4**: 201-210.

Schultz, A., 1989, "Variability of fluid temperature, velocity, and heat flux from diffuse hydrothermal percolation, Endeavour Segment, Juan de Fuca Ridge", EOS, **70**: 1161.

Schultz, A., J. R. Delaney and R. E. McDuff, 1990, "Extended Geophysical Ovservations of Ridge Crest Hydrothermal Systems: Heat Flux and Related Quantities", EOS, **71**: 1619.

Speer, K. G., 1988, "The Influence of Geothermal Sources on Deep-Ocean Temperature, Salinity, and Flow Fields", Ph.D. Thesis, MIT/WHOI.

Speer, K. G. and P. A. Rona, 1989, "A Model of an Atlantic and Pacific Hydrothermal Plume", Journal of Geophysical Research, **94**: 6213-6220.

Sturgeon, R. E., S. S. Berman, A. Desaulniers and D. S. Russell, 1980, "Pre-concentration of trace metals from sea-water for determination by graphite furnace atomic-absorption spectrometry", Talanta, **27**: 85-94.

Sturgeon, R. E., S. S. Berman, S. N. Willie and J. A. H. Desaulniers, 1981, "Preconcentration of trace metals from seawater with silica-immobilized 8-hydroxyquinoline", Analytical Chemistry, **53**: 2337-2340.

Sung, W. and J. J. Morgan, 1981, "Oxidative removal of Mn(II) from solution catalysed by the γ-FeOOH (lepidocrocite) surface", Geochimica et Cosmochimica Acta, **45**: 2377-2383.

Tivey, M. K. and J. R. Delaney, 1986, "Growth of large sulfide structures on the Endeavour Segment of the Juan de Fuca Ridge", Earth and Planetary Science Letters, **77**: 303-317.

Trefry, J. H., R. P. Trocine, G. P. Klinkhammer and P. A. Rona, 1985, "Iron and copper enrichment of suspended particles in dispersed hydrothermal plumes alomg the Mid-Atlantic Ridge", Geophysical Research Letters, **12**: 506-509.

Trocine, R. P. and J. H. Trefry, 1988, "Distribution and chemistry of suspended particles from an active hydrothermal vent site on the Mid-Atlantic Ridge at 26 °N", Earth and Planetary Science Letters, **88**: 1-15.

Turner, J. S., 1969, "Buoyant Plumes and Thermals", Annual Review of Fluid Mechanics, **1**: 29-44.

Turner, J. S. and I. H. Campbell, 1987, "Temperature, density, and buoyancy fluxes in "black smoker" plumes, and the criterion for buoyancy reversal", Earth and Planetary Science Letters, **86**: 85-92.

Turner, J. S. and L. B. Gustafson, 1978, "The Flow of Hot Saline Solutions from Vents in the Sea Floor - Some Implications for Exhalative Massive Sulfide and Other Ore Deposits", Economic Geology, **73**: 1082-1100.

Von Damm, K. L. and J. L. Bischoff, 1987, "Chemistry of Hydrothermal Solutions From the Southern Juan de Fuca Ridge", Journal of Geophysical Research, **92**: 11334-11346.

Von Damm, K. L., J. M. Edmond, B. Grant, C. I. Measures, B. Walden and R. F. Weiss, 1985a, "Chemistry of submarine hydrothermal solutions at 21 °N, East Pacific Rise", Geochimica et Cosmochimica Acta, **49**: 2197-2220.

Von Damm, K. L., J. M. Edmond, C. I. Measures and B. Grant, 1985b, "Chemistry of submarine hydrothermal solutions at Guaymas Basin, Gulf of California", Geochimica et Cosmoshimica Acta, **49**: 2221-2237.

Walker, S. L. and E. T. Baker, 1988, "Particle-size distributions within hydrothermal plumes over the Juan de Fuca Ridge", Marine Geology, **78**: 217-226.

Weiss, R. F., 1977, "Hydrothermal manganese in the deep sea: Scavenging residence time and Mn/3He relationships", Earth and Planetary Science Letters, **37**: 257-262.

Welhan, J. A. and H. Craig, 1983, "Methane, Hydrogen, and Helium in Hydrothermal Fluids at 21° N on the East Pacific Rise", in Hydrothermal processes at seafloor spreading centers, 391-410.

Winn, C. D., D. M. Karl and G. J. Massoth, 1986, "Microorganisms in deep-sea hydrothermal plumes", Nature, **320**: 744-746.

APPENDICES

APPENDIX A: Manganese Analysis Method

Reagent Preparation

All of the following work was carried out under Class 100 laminar flow hoods to minimize the risk of contamination. Analytical reagent grade (Mallinckrodt) 8-hydroxyquinoline was purified by vacuum sublimation at 120° C onto a cleaned glass cold finger cooled with tap water (Sturgeon, et al., 1980; Sturgeon, et al., 1981). Approximately 0.5 g of the purified 8-hydroxyquinoline was added to 500 ml of Omnisolve spectophotometric grade chloroform to make the extraction solvent (8-HQ/CCl_3H). A 0.125 M sodium borate buffer was run through a Chelex resin bed to remove trace metal impurities. A 2.8% NaOH solution was used to raise the pH of the seawater samples.

Sample Extraction

The efficiency of the extraction is highly dependent on pH, with optimum results being obtained at pH 9. Control of the pH was greatly improved by the addition of a chelexed, concentrated sodium borate buffer solution. Approximately 15 ml (15.5 g) of sample were pipetted into a 40 ml teflon Oak-Ridge type, centrifuge tube. Centrifuge tube weights were recorded before and after the addition to obtain the sample weights. The pH of the samples was raised from <2 to ~9.0 (± 0.1) by the addition of ~200 µl of 2.8% NaOH and buffered by the addition of 200 µl of 0.125 M sodium borate. 5 ml of 8-HQ/CCl_3H were added to each sample, and the tubes were vortexed for 5 minutes and allowed to settle for 5 minutes. The lower organic layer was removed to another tube which contained 5 ml of 3 N HNO_3 (subboiling-distilled). 5 ml of 8-HQ/CCl_3H were again added to the sample and the extraction step repeated. The organic layer was again removed to the tube containing the 3 N HNO_3. The pH of the extracted seawater was determined. If the pH was out of the 8.9 to 9.1 range the sample was repeated in a later analysis, changing the amount of 2.8% NaOH added to bring the pH in the desired range. The tube with the HNO_3 and the 8-HQ/CCl_3H was

vortexed for 5 minutes and allowed to settle for 5 minutes. This step back-extracted the manganese into the 3 N HNO_3. The 8-HQ/CCl_3H layer was discarded and the acid layer was poured into a 3rd centrifuge tube. The second tube was rinsed with 2 ml of 3 N HNO_3 which was then added to the 3rd centrifuge tube. The acid backextracts were then slowly evaporated at 105° C in a teflon-coated evaporation block. The solid residue was redissolved in 1 ml of 16 N HNO_3 (subboiling-distilled) and evaporated to dryness three times. This step reduces the matrix effects of the organics from the 8-HQ/CCl_3H. After the 3rd evaporation, the solid residue was redissolved in 1 ml of 3 N HNO_3 and stored under refridgeration in a 1.5 ml microcentrifuge tube for later analysis on the atomic absorption spectrophotometer.

Atomic Absorption Analysis

The samples from the microcentrifuge tubes were diluted 1:5 by adding 100 µl of sample to 400 µl of 0.16 N HNO_3 (subboiling-distilled) in a 1.5 ml polyethylene AA cup. The cups were placed on the AS-40 Autosampler tray and analyzed according to the following parameters and furnace program:

1. Sample volume = 25 µl
2. Wavelength = 279.5 nm
3. Slit width = 0.2 nm, low
4. Integration time = 5 seconds, peak height mode
5. Purge gas = argon
6. Expansion = 10X, concentration mode
7. 3 replicates

Furnace program:

	Step						
	#1	#2	#3	#4	#5	#6	#7
	dry	dry	dry	char	atom.	clean	cool
temp., °C	110	150	300	800	2200	2600	20
ramp, sec.	5	30	10	10	0	1	1
hold, sec.	1	20	15	20	5	5	4
record,sec.				21	√	√	√
read, sec					√		
baseline,sec				23			
internal flow (ml/min)	300	300	300	300	30	300	300

Data Reduction

The detection limit of the method is ~2 nmole/kg. The detection limit could be reduced by using a larger sample or lower final dilutions. Blanks were below the detection limit. Precision of the method was ~5%. Extraction efficiency was measured by extracting chelexed seawater, spiking it with known concentrations of manganese and carrying the standards through the evaporation and redissolution process. This is, in effect, a standard additions experiment. A consistency standard was made by adding manganese to acidified, chelexed seawater. This standard was analyzed twice in every extraction procedure. Its manganese concentration (calculated by comparison to the standard additions samples) was divided by the known manganese concentration to get the extraction efficiency. Long-term efficiency was ~96 (±5)%.

APPENDIX B: Hydrocast Station Profiles

Figure 20. P2CTD1 (Vent Field) profiles: (A) ΔL (m^{-1}) and ΔT (°C), (B) total and dissolved Mn (nmoles/kg), (C) total and dissolved Fe (nmoles/kg).

Figure 20 - P2CTD1 (Vent Field) Profiles

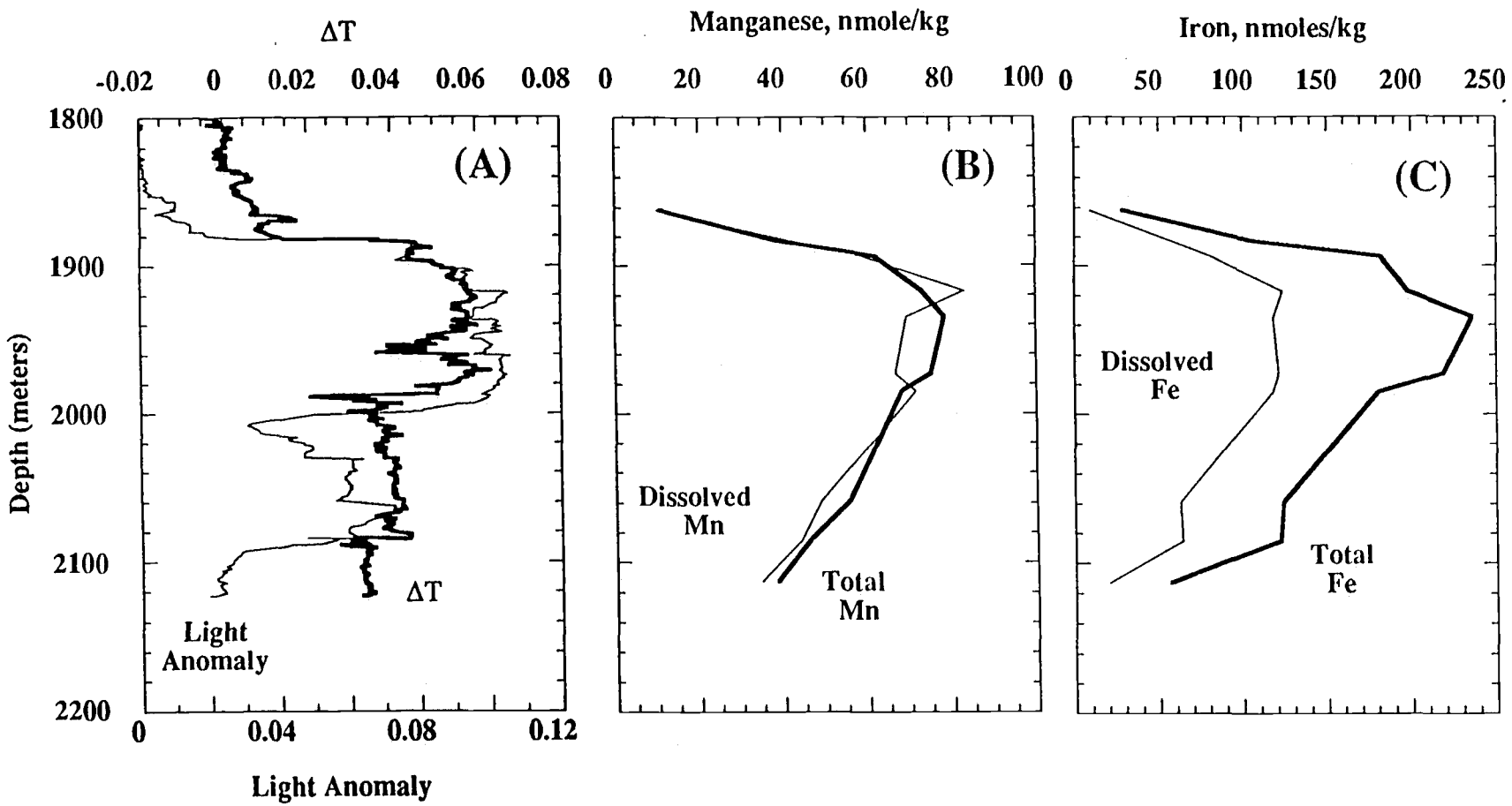

Figure 21. P2CTD3 (Vent Field) profiles: (A) ΔL (m^{-1}) and ΔT (°C), (B) total and dissolved Mn (nmoles/kg), (C) total and dissolved Fe (nmoles/kg).

Figure 21 - P2CTD3 (Vent Field) Profiles

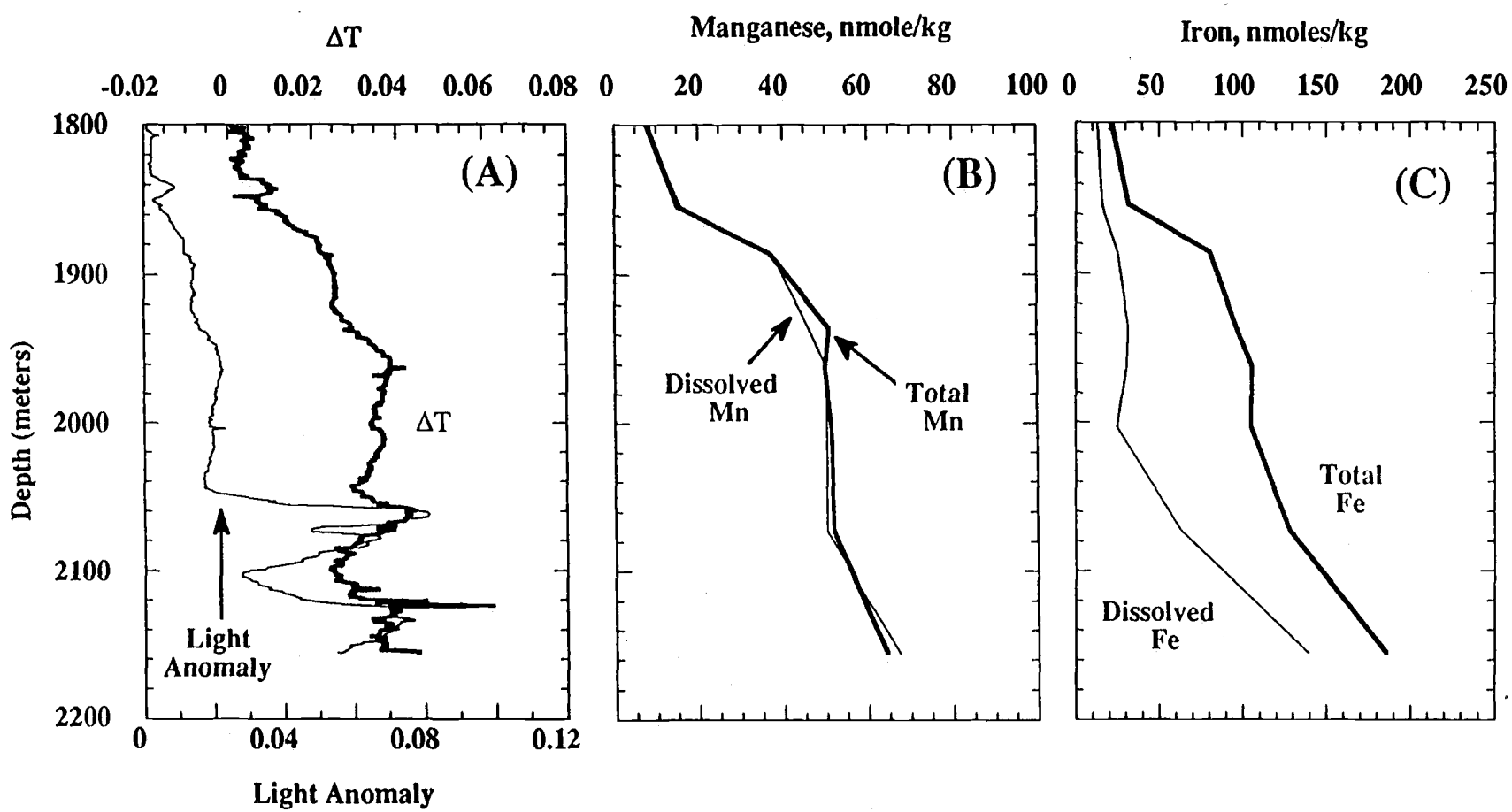

Figure 22. P2CTD12 (Vent Field) profiles: (A) ΔL (m^{-1}) and ΔT (°C), (B) total Mn (nmoles/kg).

Figure 22 - P2CTD12 (Vent Field) Profiles

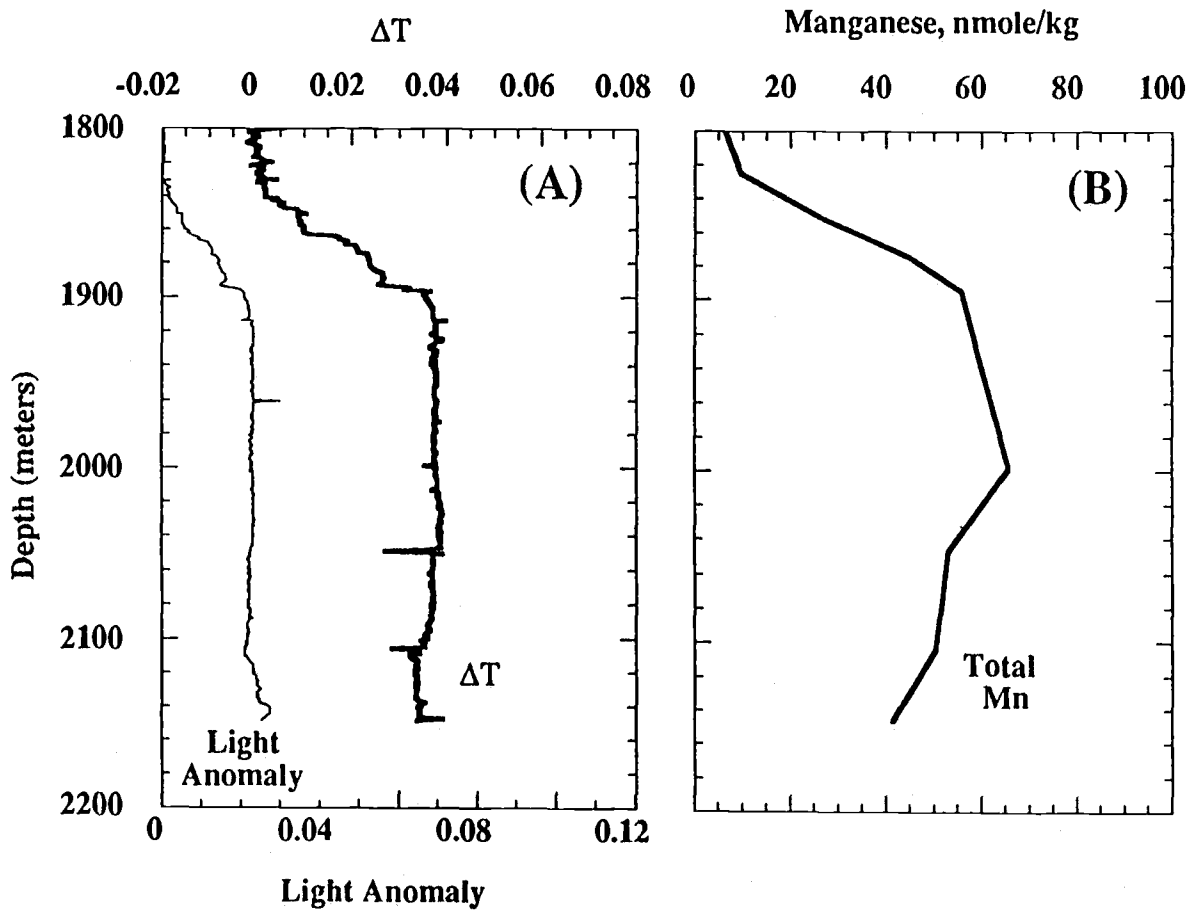

Figure 23. P2CTD15 (Vent Field) profiles: (A) ΔL (m^{-1}) and ΔT (°C), (B) total and dissolved Mn (nmoles/kg).

Figure 23 - P2CTD15 (Vent Field) Profiles

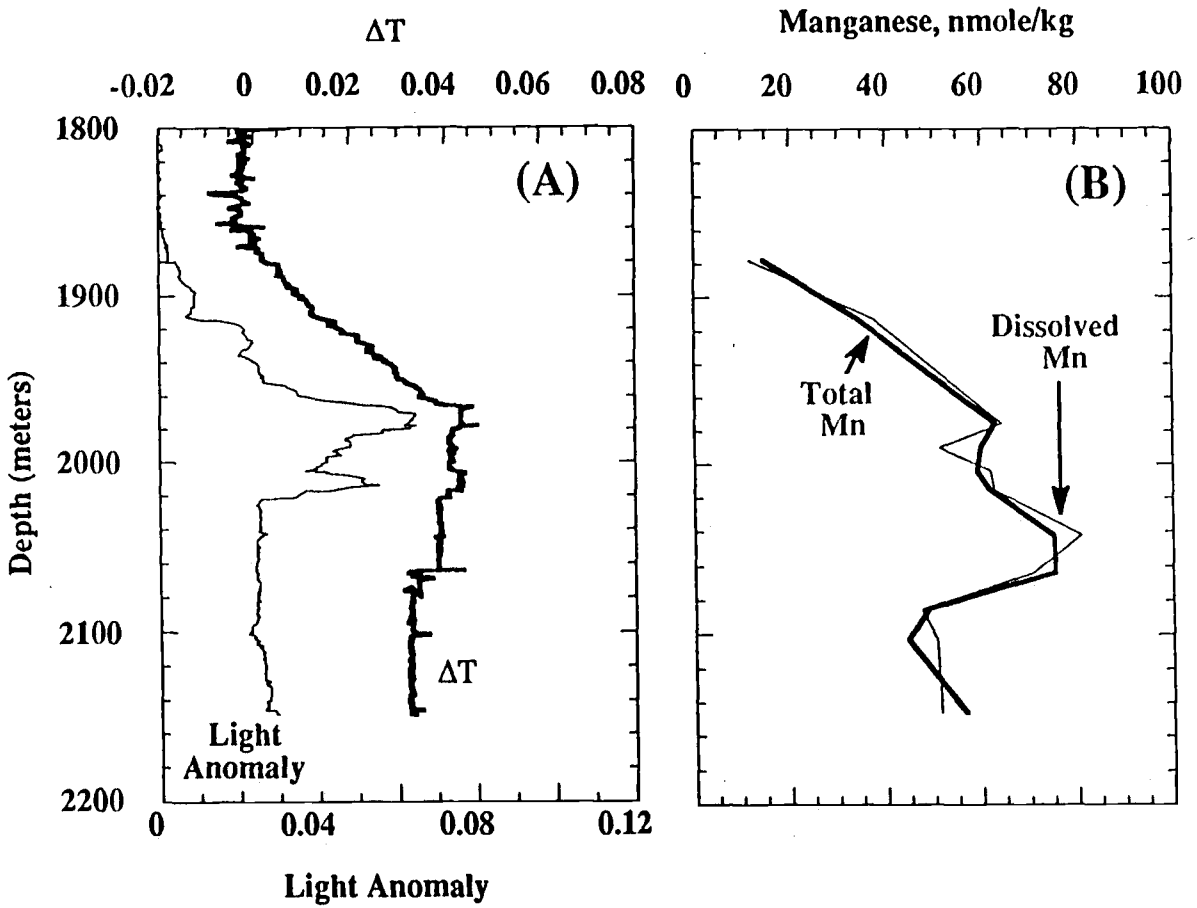

Figure 24. P2CTD9 (2 km) profiles: (A) ΔL (m^{-1}) and ΔT (°C), (B) total and dissolved Mn (nmoles/kg), (C) total and dissolved Fe (nmoles/kg).

Figure 24 - P2CTD9 (2 km) Profiles

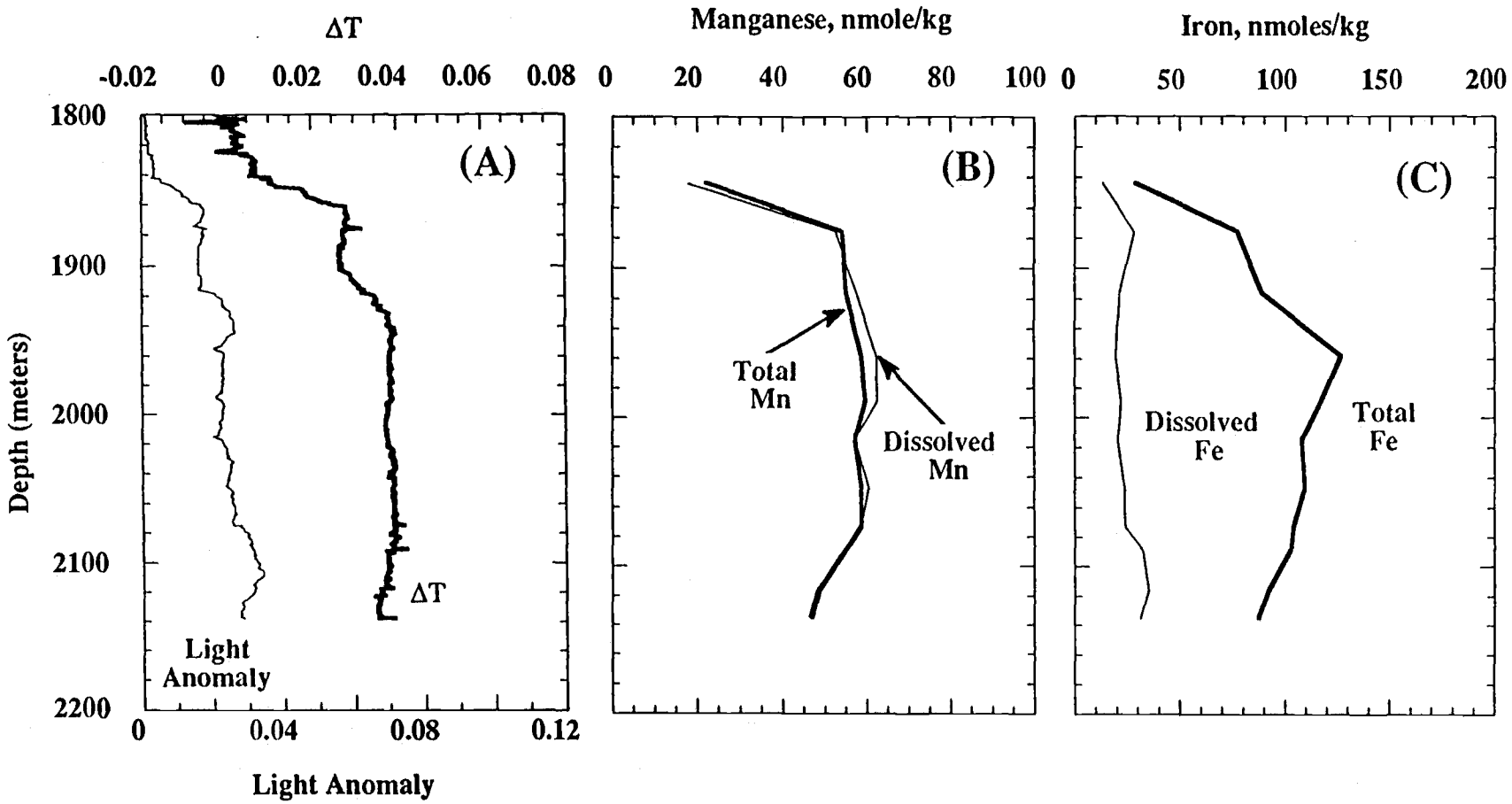

Figure 25. P2CTD4 (4 km) profiles: (A) ΔL (m^{-1}) and ΔT (°C).

Figure 25 - P2CTD4 (4 km) Profiles

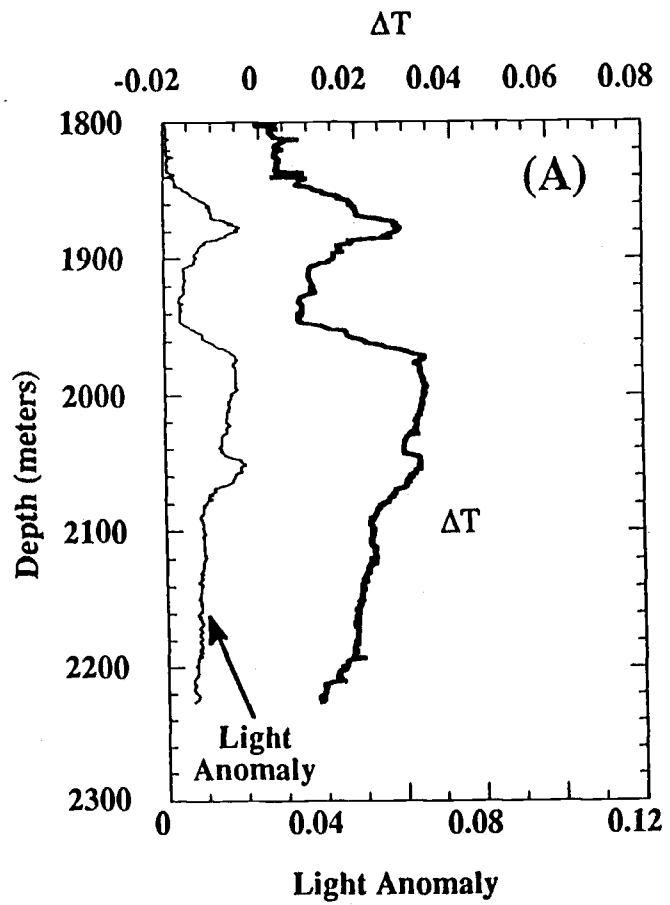

Figure 26. P2CTD6 (4 km) profiles: (A) ΔT (°C), (B) total and dissolved Mn (nmoles/kg), (C) total and dissolved Fe (nmoles/kg).

Figure 26 - P2CTD6 (4 km) Profiles

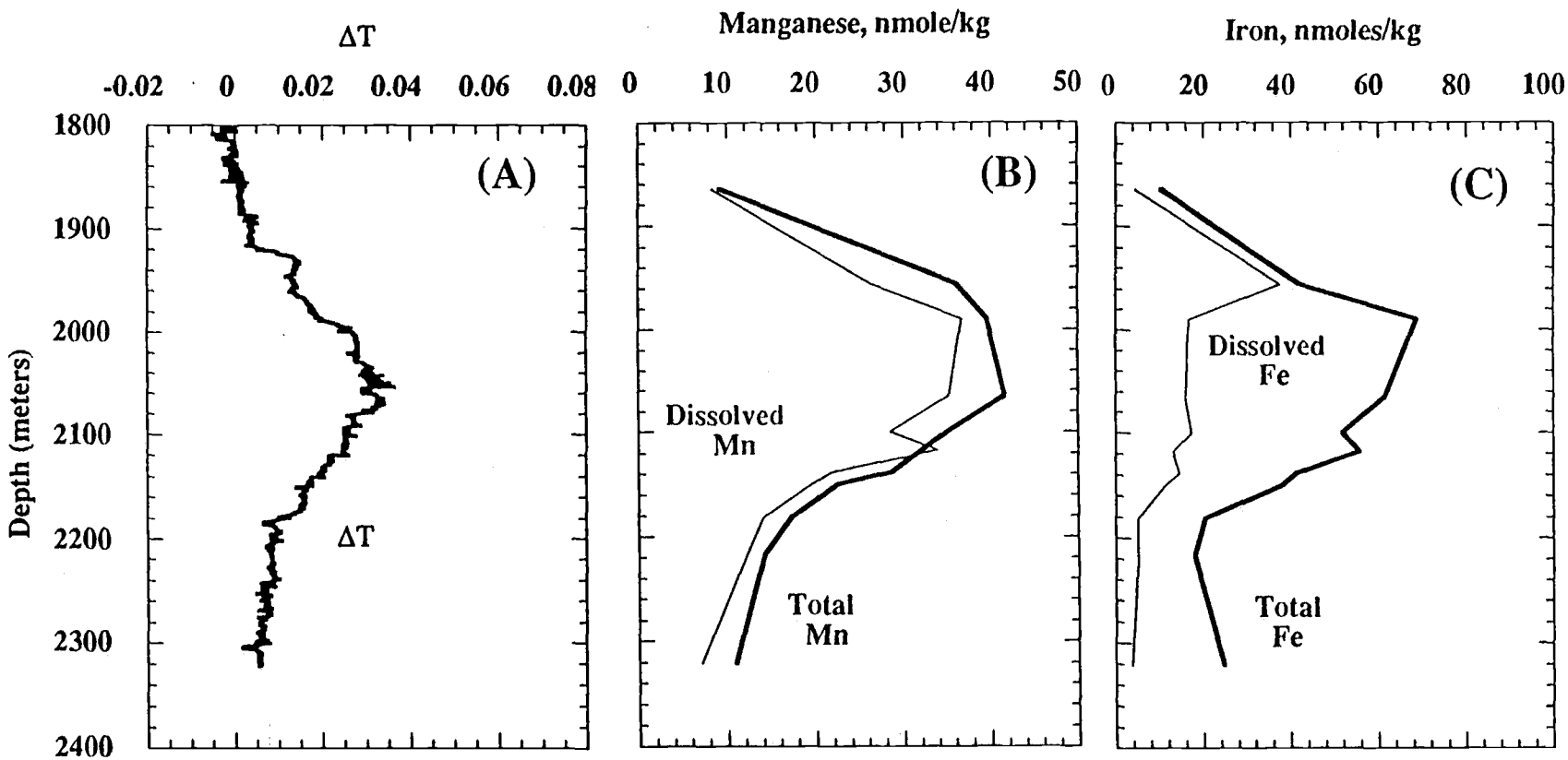

Figure 27. P2CTD10 (10 km) profiles: (A) ΔL (m^{-1}) and ΔT (°C), (B) total and dissolved Mn (nmoles/kg).

Figure 27 - P2CTD10 (10 km) Profiles

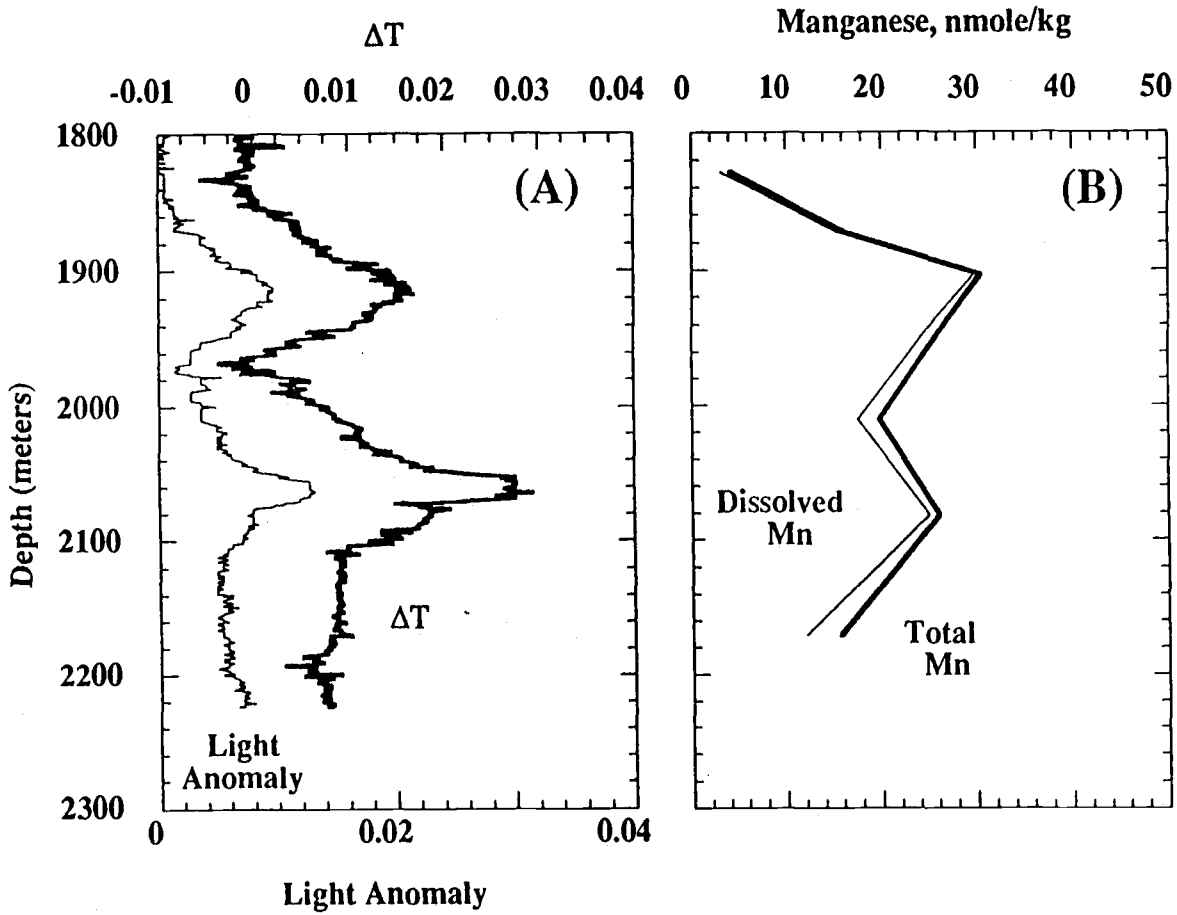

Figure 28. P2CTD11 (10 km) profiles: (A) ΔL (m^{-1}) and ΔT (°C), (B) total and dissolved Mn (nmoles/kg), (C) total and dissolved Fe (nmoles/kg).

Figure 28 - P2CTD11 (10 km) Profiles

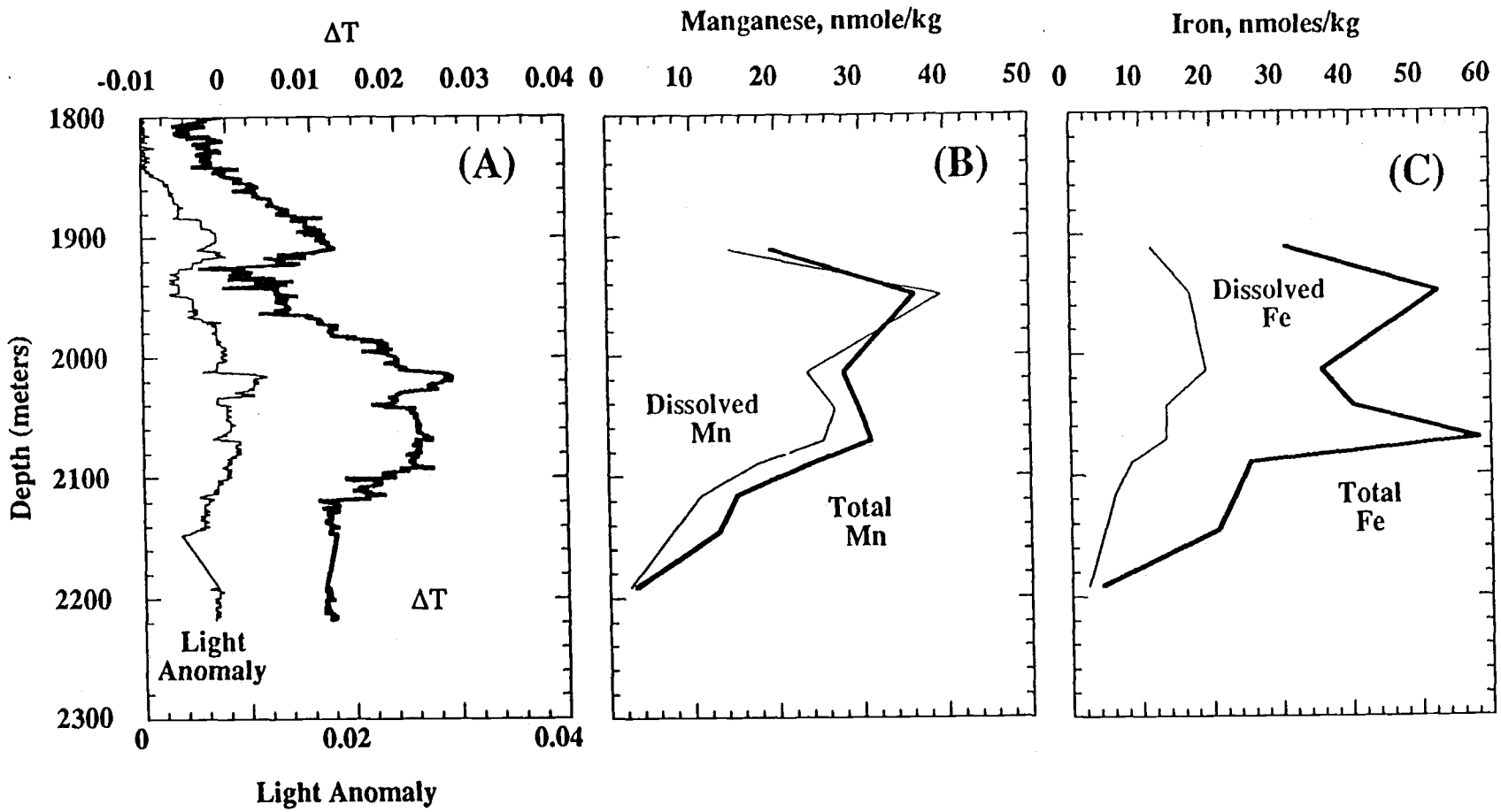

Figure 29. P2CTD16 (17 km) profiles: (A) ΔL (m^{-1}) and ΔT (°C), (B) total and dissolved Mn (nmoles/kg), (C) total and dissolved Fe (nmoles/kg).

Figure 29 - P2CTD16 (17 km) Profiles

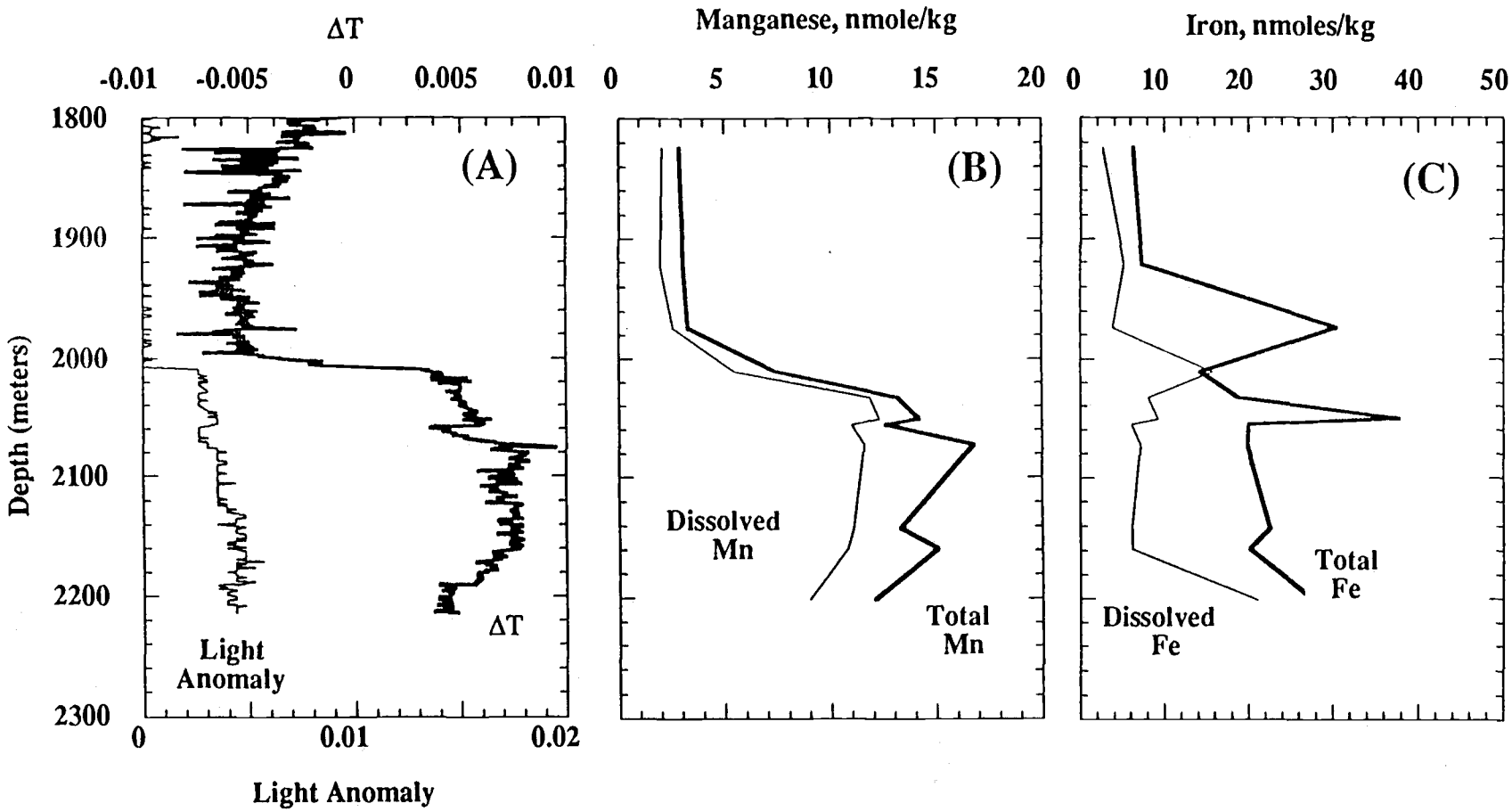

Figure 30. P2CTD18 (17 km) profiles: (A) ΔL (m^{-1}) and ΔT (°C), (B) total and dissolved Mn (nmoles/kg).

Figure 30 - P2CTD18 (17 km) Profiles

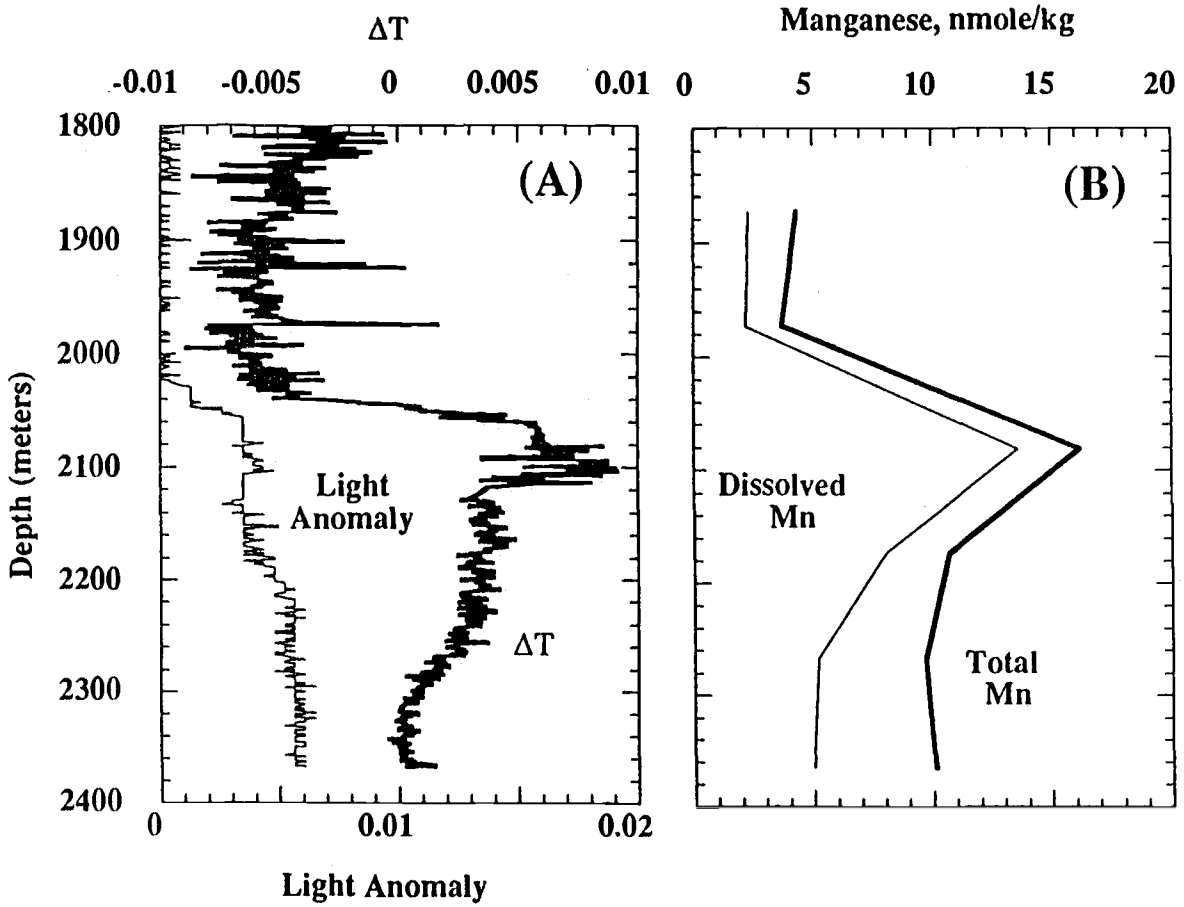

APPENDIX C: Manganese and Iron Fluxes

Dymond and Roth, 1988 measured a manganese flux of approximately 7 $\mu g/cm^2/yr$ and an iron flux of approximately 4500 $\mu g/cm^2/yr$ in an 8-day deployment of a sediment trap located within the Endeavour Ridge vent field. These fluxes represent an insignificant loss from the neutrally buoyant plume. If I assume that the water column is 250 m in height and the average velocity is 1 cm/sec, then the flux of water through an area 250 m by 1 cm is:

$$250\ m \times \frac{100\ m}{cm} \times 1\ cm \times \frac{1\ cm}{sec} \times \frac{1\ L}{1000\ cm^3} = \frac{25\ L}{sec}$$

If the manganese flux is 7 $\mu g/cm^2/yr$ (4×10^{-15} moles/cm^2/sec) and is constant over an area of 1 km by 1 cm (10^5 cm^2), then the loss from the advecting plume required to make up this loss is:

$$\frac{4 \times 10^{-15}\ moles}{cm^2 \cdot sec} \times 10^5\ cm^2 \times \frac{sec}{25\ L} = \frac{1.6 \times 10^{-11}\ moles\ Mn}{L}$$

The same calculation for an iron flux of 4500 $\mu g/cm^2/yr$ yields a loss of 1.0×10^{-8} moles Fe/L. This is approximately 5% of the 200+ nmoles Fe/L in the neutrally buoyant plume. However, this value is an overestimate, as the flux is assumed to remain constant over a 1 km distance.